SLAC–PUB–4368
July 1987
T/E

An Analysis of Quark Mass Matrices and $B - \bar{B}$ Mixing*

YOSEF NIR

Weizmann Institute of Science, Rehovot, Israel

and

Stanford Linear Accelerator Center
Stanford University, Stanford, California, 94305

ABSTRACT

We study the implications of the recent $B_d - \bar{B}_d$ mixing data on the quark sector parameters - m_t, s_{13} and δ - within the three generation standard model. We derive limits on several experimental quantities: r_s, ϵ'/ϵ, branching ratios of rare K and B decays. The Fritzsch scheme for quark mass matrices is consistent with the experimental data only if several experimental and theoretical quantities assume values at the limit of their allowed ranges. This allows a unique solution: $m_t \sim 85\ GeV$, $s_{13} \sim 0.035$, $\delta \sim 100°$, with many definite predictions. The Stech scheme and its extension by Gronau, Johnson and Schechter are inconsistent with the experimental constraints. We study how a direct measurement of m_t or s_{13} will improve our constraints and predictions.

Submitted to Nuclear Physics

---

* Work supported by the Department of Energy, contract DE–AC03–76SF00515.

1. Introduction

The standard model with three generations of fermions has undergone numerous experimental tests. All these tests have confirmed again and again the validity of the standard model predictions of low-energy phenomena. The predictions of the *minimal* standard model can all be given in terms of eighteen independent parameters. Of these, ten are related to the quark sector of the theory.

The ten parameters describing the quark sector of the three generation standard model consist of *six quark masses, three mixing angles and one Kobayashi-Maskawa (KM) phase.* The quark masses are best determined from meson spectroscopy and chiral perturbation theory. The mixing angles are best determined from flavor changing tree level decays of mesons. We call these *"direct" measurements.* Further information on the value of the parameters comes from processes that occur only at the loop level of the standard model. We call such information *"indirect" measurements.*

Seven of the quark sector parameters are relatively well known. These are five of the quark masses (given here in GeV):

$$\begin{aligned} m_d &\sim 0.009 \ ; \ m_s \sim 0.15 \ ; \ m_b \sim 5 \\ m_u &\sim 0.005 \ ; \ m_c \sim 1.5 \end{aligned} \tag{1.1}$$

and two of the mixing angles:

$$s_{12} \sim 0.22 \ ; \ s_{23} \sim 0.05 \tag{1.2}$$

We gave here only the order of magnitude of these parameters. Later we comment on the accuracy of our knowledge of some of them. All the above values result from direct measurements.

Three parameters are rather poorly determined. The top quark has not yet been found. There is a lower limit on its mass, coming from its non-observation in

e^+e^- anihilations: $m_t \geq 23\ GeV$. If the difference between the sqaured masses of the t-quark and the b-quark were too large, the predicted value of $\sin^2\theta_W$ would deviate too much from its measured value. This gives [1] $m_t \leq 180\ GeV$. We will refer to the bounds

$$23\ GeV \leq m_t \leq 180\ GeV \tag{1.3}$$

as "direct" bounds, although the upper limit comes from an indirect measurement. The third mixing angle, s_{13}, has only a direct *upper* limit on its value

$$s_{13} \leq 0.011 \tag{1.4}$$

We will later explain how this limit is determined. The phase δ has only very loose bounds on its value, coming from the measurement of the CP-violating parameter ϵ.

Recently, the ARGUS collaboration has found a positive evidence for $B_d - \bar{B}_d$ mixing [2]. This result significantly contributes to our knowledge of the quark sector parameters. The combination of the $B - \bar{B}$ mixing data and of the ϵ value gives constraints on the allowed values of the three poorly determined parameters. In the near future, a large amount of additional information is expected to be found from further studies of B physics. Another possible source of information is the continuous search for the top quark. The first purpose of this paper is to analyze the implications of the existing ARGUS data on the quark sector parameters and to understand how near future experiments will further restrict the allowed domain of these parameters.

The implications of the $B - \bar{B}$ mixing data on the standard model parameters were previously discussed in several papers [3 – 6]. We here give a much more detailed analysis and a broader scope of results.

In the standard model, mixing angles and quark masses are unrelated. Several models beyond the standard model suggest special forms of mass matrices.

These mass matrices have less than ten independent parameters, thus giving relations among quark masses, mixing angles and phases. Consequently, they are more constrained than the standard model, and one could check if their predictions are consistent with the experimental values of the quark sector parameters. In this paper we consider four such schemes: the Fritzsch scheme [7] with eight independent parameters, the Stech scheme [8] with seven independent parameters, the Fritzsch-Shin scheme [9] and the Gronau-Johnson-Schechter (GJS) scheme [10], each with six independent parameters. We check whether the predictions of these mass matrices are consistent with the new ARGUS results and with all earlier data. For the schemes which do not fail to account for the observed $B-\bar{B}$ mixing, we study their predictions for the results of future experiments.

The general lines of our calculations and our main results were given in a previous paper [5]. Here we give the details of these calculations, a much more detailed explanation of the different considerations and additional results and predictions.

The paper is organized as follows: In chapter 2 we describe the constraints on the quark sector parameters. We emphasize the ambiguities involved in inferring values for s_{23} and s_{13} from direct measurements. We review the constraints on m_t, s_{13} and δ coming from the ϵ measurement, and carefully analyze those resulting from the $B-\bar{B}$ mixing measurement. In chapter 3 we give predictions for future experiments ($B_s-\bar{B}_s$ mixing, direct CP violation and rare K and B decays), based on the allowed range of parameters derived in chapter 2. In chapter 4 we present the different schemes for quark mass matrices that we study. We explain the relations between the *"physical"* quark masses (involved in the physical processes which serve as measurements for mixing angles) and *"running"* quark masses (which appear in the mass matrices). In chapter 5 we study the consistency of the Fritzsch scheme (and its extension by Shin) with the new experimental data. In chapter 6 we study the consistency of the Stech scheme (and its extension by GJS) with these data. In chapter 7 we give our conclusions, and describe further experimental tests expected in the near future.

2. The quark mixing matrix in the standard model

2.1. PARAMETRIZATION

We use the following parametrization [11] for the CKM-matrix:

$$V = \begin{pmatrix} c_{12}c_{13} & s_{12}c_{13} & s_{13}e^{-i\delta} \\ -s_{12}c_{23} - c_{12}s_{23}s_{13}e^{i\delta} & c_{12}c_{23} - s_{12}s_{23}s_{13}e^{i\delta} & s_{23}c_{13} \\ s_{12}s_{23} - c_{12}c_{23}s_{13}e^{i\delta} & -c_{12}s_{23} - s_{12}c_{23}s_{13}e^{i\delta} & c_{23}c_{13} \end{pmatrix} \tag{2.1}$$

where $c_{ij} \equiv \cos\theta_{ij}$ and $s_{ij} \equiv \sin\theta_{ij}$. The notations follow those of ref. [12]. It is experimentally known that

a. The mixing angles are small, so that all c_{ij} fulfill $c_{ij} = 1$ to order 10^{-2}.

b. The s_{ij} fulfill $s_{12} > s_{23} > s_{13}$.

Consequently, we may use the approximation

$$V = \begin{pmatrix} 1 & s_{12} & s_{13}e^{-i\delta} \\ -s_{12} - s_{23}s_{13}e^{i\delta} & 1 & s_{23} \\ s_{12}s_{23} - s_{13}e^{i\delta} & -s_{23} & 1 \end{pmatrix} \tag{2.2}$$

The second term in V_{cd} is only relevent in the calculation of the CP-violating parameter ϵ.

2.2. "DIRECT" MEASUREMENTS

The main advantage of the parametrization (2.2) is that direct measurements of the matrix elements V_{us}, V_{cb} and V_{ub} are trivially translated into values of s_{12}, s_{23} and s_{13} (respectively).

An analysis [13] of the K_{e3} and hyperon decays gives for $s_{12} = |V_{us}|$:

$$s_{12} = 0.220 \pm 0.002 \tag{2.3}$$

The value of $s_{23} = |V_{cb}|$ can be extracted from the semileptonic B-meson partial width [14 – 18]. One assumes that it is given by the b-quark W-mediated

decay:

$$\Gamma(b \to c\ell\bar{\nu}_\ell) = \frac{G_F^2 m_b^5}{192\pi^3} F(m_c^2/m_b^2)|V_{cb}|^2 \tag{2.4}$$

where $F(m_c^2/m_b^2)$ is a phase space factor:

$$F(x) = 1 - 8x + 8x^3 - x^4 - 12x^2 \ln(x) \tag{2.5}$$

Thus, $(s_{23})^2$ is given by

$$(s_{23})^2 = \left[\frac{192\pi^3}{G_F^2}\right]\left[\frac{BR(b \to c\ell\bar{\nu}_\ell)}{\tau_b}\right]\left[\frac{1}{m_b^5 F(m_c^2/m_b^2)}\right] \tag{2.6}$$

We use the experimental data [17]

$$BR(b \to c\ell\bar{\nu}_\ell) = 0.121 \pm 0.008 \tag{2.7}$$

and [18]

$$\tau_b = (1.16 \pm 0.16) \times 10^{-12}\ sec \tag{2.8}$$

The quark masses m_b and m_c that should be used in our different calculations are subject to many theoretical uncertainties [15, 17]. We take these uncertainties into consideration by allowing for large errors:

$$m_c = 1.5 \pm 0.2\ GeV\ ;\ m_b = 5.0 \pm 0.3\ GeV \tag{2.9}$$

However, it is unlikely that in any single calculation we should use m_c and m_b at their *opposite* limits. The meson masses are close to the respective upper limits in eq. (2.9), while the physical quark masses are close to the lower limits. Thus,

for the *ratio* m_c/m_b, relevant to eq. (2.6), we take a smaller range:

$$m_c/m_b = 0.30 \pm 0.03 \tag{2.10}$$

Using the full range of the ratio (2.10) we get:

$$F(m_c^2/m_b^2) = 0.52 \pm 0.07 \tag{2.11}$$

The determination of s_{23} from the B-meson semileptonic decay (eq. (2.6)) is thus subject to both experimental and theoretical uncertainties. Due to the m_b^5-dependence, we cannot determine $(s_{23})^2$ to an accuracy better than 30%. Adding the errors in quadrature we get

$$(s_{23})^2 = (1.85 \pm 0.65) \times 10^{-3} \tag{2.12}$$

which gives

$$s_{23} = 0.043^{+0.007}_{-0.009} \tag{2.13}$$

One may argue that while the *amplitude* for the decay is reasonably described at the *quark* level, the *phase space factor* should be calculated with the *meson* masses: $m_b \approx M_B$ and $M_D \leq m_c \leq M_{D^*}$. Both m_b and m_c/m_b are larger than the values we used before. Consequently, the value of the relevant factor $m_b^5 F(m_c^2/m_b^2)$ does not change much. Allowing the full range of $BR(b \to c\ell\bar{\nu}_\ell)$ and τ_b we get:

$$\begin{aligned} 0.35 \leq & F(m_c^2/m_b^2) \leq 0.40 \\ 0.038 \leq & \ s_{23} \ \leq 0.050 \end{aligned} \tag{2.14}$$

As this calculation gives s_{23} values within our former bounds (2.13), we may safely use eq. (2.13) as our bounds. As for the lower range of $F(m_c^2/m_b^2)$ derived using meson masses, all our calculations (other than the above s_{23} calculation) use only the upper limit on $F(m_c^2/m_b^2)$. Thus we may safely use eq. (2.11) for these calculations.

Recent measurements tend to give τ_b-values closer to the lower limit in eq. (2.8). This may eventually lead to somewhat higher s_{23} values.

The non-observation of charmless B-decays [17],

$$\frac{\Gamma(b \to u\ell\bar{\nu}_\ell)}{\Gamma(b \to c\ell\bar{\nu}_\ell)} \leq 0.08, \tag{2.15}$$

gives an upper bound on $s_{13} = |V_{ub}|$:

$$s_{13} \leq [0.08\ F(m_c^2/m_b^2)]^{1/2} s_{23} \tag{2.16}$$

In order to avoid the large uncertainties involved in the determination of s_{23}, we will use the the ratio between s_{13} and s_{23} rather than s_{13} itself:

$$q \equiv \frac{|V_{ub}|}{|V_{cb}|} = \frac{s_{13}}{s_{23}} \leq [0.08\ F(m_c^2/m_b^2)]^{1/2} \leq 0.22 \tag{2.17}$$

where we used $F(m_c^2/m_b^2) \leq 0.59$. As $s_{23} \leq 0.050$,

$$s_{13} \leq 0.011 \tag{2.18}$$

This bound strengthens the validity of the approximation we made while replacing $|V_{us}|$, $|V_{cb}|$ and $|V_{ub}|$ with s_{12}, s_{23} and s_{13}: this approximation is actually good to order 10^{-4}.

Recent measurements [19] suggest an upper bound which is more stringent than the one in eq. (2.15). Thus, our use of the bound (2.17) may be regarded as conservative.

To summarize: Direct measurements give

$$s_{12} = 0.220 \pm 0.002 \ ; \ s_{23} = 0.043^{+0.007}_{-0.009} \ ; \ s_{13} \leq 0.011 \tag{2.19}$$

We will often use

$$(s_{23})^2 = (1.85 \pm 0.65) \times 10^{-3} \ ; \ q = \frac{s_{13}}{s_{23}} \leq 0.22 \tag{2.20}$$

2.3. "INDIRECT" MEASUREMENTS

The experimental results that we use to further limit the allowed range of the quark sector parameters are the measurements of the CP-violating parameter ϵ, and the $B - \bar{B}$ mixing parameter x_d. The standard model contributions to these parameters come from box diagrams and are GIM-suppressed. *Relating these experimental results to the CKM parameters depends on the assumption that there are no significant contributions from diagrams beyond the standard model.*

<u>CP-violation: ϵ</u> The expression for ϵ [20] with the parametrization (2.2) is

$$|\epsilon| = C \cdot B_K \cdot [s_{23}]^2 q \sin\delta \left\{ [\eta_3 f_3(y_t) - \eta_1] y_c s_{12} + \eta_2 y_t f_2(y_t) (s_{23})^2 [s_{12} - q\cos\delta] \right\} \tag{2.21}$$

where

$$\begin{aligned} y_i =& \frac{m_i^2}{M_W^2} \quad (i = c, t) \\ f_2(y_t) =& 1 - \frac{3}{4} \frac{y_t(1+y_t)}{(1-y_t)^2} \left[1 + \frac{2y_t}{1-y_t^2} \ln(y_t) \right] \\ f_3(y_t) =& \ln\left(\frac{y_t}{y_c}\right) - \frac{3}{4} \frac{y_t}{1-y_t} \left[1 + \frac{y_t}{1-y_t} \ln(y_t) \right] \\ C \equiv& \frac{G_F^2 f_K^2 M_K M_W^2}{6\pi^2 \sqrt{2} \Delta M_K} \end{aligned} \tag{2.22}$$

Eq. (2.21) gives a relation among the three undetermined parameters of the quark sector, (m_t, q, δ). Other parameters in eq. (2.21) may be divided into two groups:

a. Parameters which are known to a high accuracy (uncertainties of a few percent or less). These are s_{12} (eq. (2.3)) and

$$\begin{aligned} |\epsilon| =& 2.3 \times 10^{-3} \\ C =& 4 \times 10^4 \\ \eta_1 =& 0.7 \ ; \ \eta_2 = 0.6 \ ; \ \eta_3 = 0.4 \end{aligned} \tag{2.23}$$

The three parameters η_i are QCD corrections [21]. The dimensionless con-

stant C was calculated using

$$G_F = 1.166 \times 10^{-5}\ GeV^{-2};\quad M_W = 82\ GeV$$
$$f_K^2 = (0.16\ GeV)^2;\quad M_K = 0.498\ GeV;\quad \Delta M_K = 3.52 \times 10^{-15}\ GeV \tag{2.24}$$

b. Parameters with large uncertainties. These are m_c (eq. (2.9)), $(s_{23})^2$ (eq. (2.12)) and the B_K parameter, which is usually estimated to be in the range

$$\frac{1}{3} \leq B_K \leq 1. \tag{2.25}$$

Either or both of m_t and q may be soon directly measured. Thus, we present the "ϵ-relation" (eq. (2.21)) in two ways:

(*i*) We fix m_t and get a curve in the $q - \delta$ plane. We show two examples in fig. (1.a): in order to demonstrate the ϵ-relation for both low and high values of m_t we select $m_t = 55\ GeV$ and $m_t = 120\ GeV$. We take here $B_K = 1$. Using the central values, $s_{23} = 0.043$ and $m_c = 1.5\ GeV$, we get the central curve. Taking the maximal values, $s_{23} = 0.050$ and $m_c = 1.7\ GeV$, gives a lower bound on q, while taking minimal values, $s_{23} = 0.034$ and $m_c = 1.3\ GeV$, gives an upper bound. Values of (δ, q) within the band (and below $q = 0.22$) are allowed. Comparing the two m_t values, one can see that the higher m_t, the lower the curves.

(*ii*) We fix q and get a curve in the $m_t - \delta$ plane. We show two examples in fig. (1.b): we choose $q = 0.20$ and 0.06 to show the ϵ-relation for high and low q-values. Again, we take $B_K = 1$. Taking for s_{23} and m_c the central, maximal or minimal values, give the central curve, a lower bound and an upper bound on m_t, respectively. The region within the bounds and with $23\ GeV \leq m_t \leq 180\ GeV$ is allowed. Lower q-values give higher curves.

We studied the implications of the ϵ relation for the whole range of m_t and q in a similar manner to the one given in the above examples. Additional examples

are given in figs. (4)-(9) (together with information from the x_d data). We derived the following conclusions:

a. The ϵ-bounds by themselves do not exclude any range of m_t within the direct bounds. Values of q below 0.02, and values of δ below 20^o (and above 178^o) are excluded.

b. Smaller B_K values raise the ϵ curves (in both the $q-\delta$ plane and the $m_t-\delta$ plane), thus strengthening the lower bounds and weakening the upper bounds.

c. The upper bound on q is more stringent than the direct bound only for large m_t. The upper bound on m_t is more stringent than the direct bound only for large q.

All these results by themselves are known. We present them here because we will later be interested in combining these results with those derived from the new $B-\bar{B}$ mixing data.

$\underline{B-\bar{B} \text{ mixing: } x_d}$ The ARGUS collaboration has recently observed $B_d-\bar{B}_d$ mixing with [2]

$$r_d = 0.21 \pm 0.08 \tag{2.26}$$

We will use the parameter $x_d \equiv \frac{\Delta M}{\Gamma}$ which is related to r_d by:

$$r_d = \frac{x_d^2}{2+x_d^2} \tag{2.27}$$

The expression for x_d is [14, 22]:

$$x_d = \tau_b \frac{G_F^2}{6\pi^2} \eta M_B (B_B f_B^2) M_W^2 y_t f_2(y_t) |V_{td}^* V_{tb}|^2 \tag{2.28}$$

We neglect here the contributions of lighter intermediate quarks (u, c) and corrections of order $\frac{m_b^2}{m_t^2}$ due to external momenta.

Note that while $K - \bar{K}$ mixing depends on $Re[M_{12}(K^0)]$, the $B - \bar{B}$ mixing depends on $|M_{12}(B^0)|$.

In our parametrization

$$|V_{td}|^2 = (s_{23})^2 \left[s_{12}^2 + q^2 - 2s_{12}q\cos\delta\right] \tag{2.29}$$

while $|V_{tb}|^2 = 1$ to a high accuracy.

Eqs. (2.28) and (2.29) give a relation among the three parameters m_t, q, δ. Again, the other parameters in these equations may be divided into two groups:

a. Parameters which are well known. In addition to the previous parameters, G_F, M_W and s_{12}, we now use

$$M_B = 5.28\ GeV;\ \eta = 0.85 \tag{2.30}$$

where η is a QCD correction [14].

b. Parameters with large experimental errors (x_d, $\tau_b s_{23}^2$) or theoretical ambiguities ($B_B f_B^2$). From eqs. (2.26) and (2.27) we get

$$x_d = 0.73 \pm 0.18 \tag{2.31}$$

One should note that s_{23} and τ_b appear only in the combination $[\tau_b(s_{23})^2]$, which does not depend on τ_b, as can be readily seen from eq. (2.6). Therefore, the error on this combination is somewhat smaller than on $(s_{23})^2$ alone:

$$\tau_b(s_{23})^2 = (3.25 \pm 1.10) \times 10^9\ GeV^{-1} \tag{2.32}$$

where errors on the quantities in eq. (2.6) were added in quadrature. The hadronic parameter B_B (analogous to B_K of the Kaon system) is believed to be close to 1. However, there is much uncertainty involved in the calculation

of the B decay constant f_B. QCD sum rules give results which depend on the on-shell b quark mass: using $m_b = 4.26\ GeV$ gives [23] $f_B = 190 \pm 30\ MeV$, while using $m_b = 4.8\ GeV$ gives [24] $f_B = 130 \pm 15\ MeV$. Other approaches use the $B - B^*$ mass difference [25], the MIT bag model [26] and potential models [27]. They all give values in the region $50\ MeV \leq f_B \leq 150\ MeV$. We will use

$$B_B f_B^2 = (0.15 \pm 0.05\ GeV)^2 \tag{2.33}$$

We note that our constraints on the quark sector parameters strongly depend on the upper limit in eq. (2.33).

We can write:

$$x_d/C' = y_t f_2(y_t)[s_{12}^2 + q^2 - 2s_{12}q\cos\delta] \tag{2.34}$$

where:

$$C' \equiv [\tau_b(s_{23}^2)]\frac{G_F^2}{6\pi^2}\eta M_B(B_B f_B^2)M_W^2|V_{tb}|^2 = 5.1^{+7.0}_{-3.6} \tag{2.35}$$

We used here the full range of $[\tau_b(s_{23})^2]$ and $B_B f_B^2$. We will use eq. (2.34) with the numerical values (2.31) and (2.35) as our "x_d-relation" among (m_t, q, δ). As the product in eq. (2.32) does not depend on τ_b, improved measurements of the b-lifetime will not affect the x_d relation, but may - rather paradoxically - affect the ϵ-relation through a possible shift in s_{23} values.

We present the x_d relation in two ways, demonstrated in fig. (2):

(i) We select a value for m_t (again, we take as examples $m_t = 55,\ 120\ GeV$). This is shown in fig. (2.a). Using $x_d = 0.73$ and $C' = 5.1$ we get the central curve in the $q - \delta$ plane. The edges of the band are derived using $(x_d = 0.55,\ C' = 12.1)$ and $(x_d = 0.91,\ C' = 1.5)$. For the low m_t the upper bound lies far above the *direct* upper limit $q \leq 0.22$ and is not shown in the figure. For the high m_t there is no lower bound on q, namely $q = 0$

is allowed. The allowed (δ, q) values are those within the band and below $q = 0.22$.

(ii) We select a value for q. Again, we take as our examples $q = 0.20,\ 0.06$. This is shown in fig. (2.b). Using $x_d = 0.73$ and $C' = 5.1$ we get the central curve in the $m_t - \delta$ plane. A lower bound on m_t is derived from $(x_d = 0.55,\ C' = 12.1)$. An upper bound on m_t is derived from $(x_d = 0.91,\ C' = 1.5)$. For low q values the upper bound lies far above the upper limit $m_t \leq 180\ GeV$, and therefore it is not shown in the figure. The allowed (δ, m_t) values are those within the band and with $23\ GeV \leq m_t \leq 180\ GeV$.

We studied the implications of the x_d relation for the whole range of m_t and q in the method described in the above examples. Additional examples are given in figs. (4)-(9) together with the ϵ relation. Our conclusions are:

a. The x_d-bounds together with the direct upper limit on q, exclude m_t values below $42\ GeV$.

b. No range of either q or δ is excluded for all m_t-values. In particular, $q = 0;\ \delta = 0$ is an allowed solution for large enough m_t. The x_d relation by itself cannot give us direct information on CP-violation.

c. The upper bounds on m_t and on q are always less stringent than the direct bounds.

2.4. RESULTS

In the last section, we analyzed the relations among the three undetermined parameters of the quark sector, m_t, q and δ. Now we combine the "ϵ-relation" (eq. (2.21)) with the "x_d-relation" (eq. (2.34)), and require that values of the three parameters would be consistent with both simultaneously. In addition they should, of course, obey the direct limits, $23\ GeV \leq m_t \leq 180\ GeV$ and $q \leq 0.22$.

The combination of the two relations gives us:

a. Allowed values of (m_t, q, δ). These are all points within both the ϵ-band and the x_d-band, which are consistent with the direct bounds.

b. The most likely values of $(m_t,\ q,\ \delta)$. These are the intersection points of the central curves (provided they are within the direct bounds), corresponding to central values of all parameters in eqs. (2.21) and (2.34).

As an example, we take the combined information of figs. (1) and (2), and show the results in fig. (3).

With m_t fixed (fig. (3.a)) at 55 GeV the central solution lies outside the direct bounds (as is the case for all $m_t \leq 82\ GeV$). The value of q should be above 0.13 and the phase δ is in the range $105^o - 165^o$.

With $m_t = 120\ GeV$ the central solution is $q = 0.11,\ \delta = 155^o$. Values of q above 0.03 are allowed. This limit is determined by the ϵ-bound only, as is the case for $m_t \geq 100\ GeV$. The phase δ should be in the range $40^o \leq \delta \leq 175^o$.

With q fixed (fig. (3.b)) at 0.20, the central solution is $m_t = 87\ GeV,\ \delta = 162^o$. Values of m_t above 45 GeV and $35^o \leq \delta \leq 178^o$ are allowed.

With q fixed at 0.06, the central solution is $m_t = 151\ GeV,\ \delta = 138^o$. Values of m_t above 76 GeV and $25^o \leq \delta \leq 165^o$ are allowed.

As can be seen from these examples, *the x_d bounds are significant for low m_t values and for large q values.* At large m_t and small q values, most of the excluded region of parameters is a consequence of the ϵ bounds.

We use the same method to give results for several values of m_t and q. In figs. (4)-(6) we show the allowed regions in the $q-\delta$ plane for $m_t = 45,\ 65,\ 85,\ 180\ GeV$ with $B_K = 1,\ 0.7,\ 0.4$. We also give the central solutions.

In figs. (7)-(9) we show the allowed regions and the central solutions in the $m_t - \delta$ plane for $q = 0.18,\ 0.14,\ 0.10,\ 0.04$ with $B_K = 1,\ 0.7,\ 0.4$.

For each selected value of q we derive a lower bound on m_t. The collection of these points from all q values gives a curve in the $m_t - q$ plane. This curve, shown in fig. (10), can be used in two ways:

(*i*) Once we have a value for q (or an upper bound), the curve gives the lower bound on m_t.

(*ii*) Once we have a value for m_t (or an upper bound), the curve gives a lower bound on q.

If the actual q and m_t lie both on this curve, it is required that all parameters: s_{23}, m_c, x_d and $B_B f_B^2$, should simultaneously have values that correspond to their experimental or theoretical *limits*.

The collection of all central solutions gives another curve. It is more likely that we would find q and m_t on this curve, as it corresponds to central values of all parameters involved. This curve is also shown in fig. (10).

To summarize, we get the following bounds on m_t and q:

$$\begin{aligned} 43\ GeV \leq m_t \leq 180\ GeV \\ 0.02 \leq q \leq 0.22 \end{aligned} \tag{2.36}$$

However, the m_t and q-values are more likely to be found in the range

$$\begin{aligned} 83\ GeV \leq m_t \leq 180\ GeV \\ 0.04 \leq q \leq 0.22 \end{aligned} \tag{2.37}$$

The phase δ is probably in the range $108^o - 175^o$, but values as small as 20^o and as large as 178^o cannot be excluded.

3. Predictions

There are several experimental quantities that depend on the values of the unknown parameters (m_t, q, δ). However, at present they cannot constrain these parameters for two possible reasons: Either the theoretical calculations of these quantities involve additional uncertainties, or the experiments have not yet reached the needed level of sensitivity. Thus, instead of getting *constraints* we give here *predictions* for these processes, based on the bounds that we derived.

3.1. $B_s - \bar{B}_s$ MIXING: x_s

Although the calculation of both x_d and x_s is subject to large uncertainties, the ratio between these quantities is expected to be well-approximated by

$$\frac{x_s}{x_d} = \frac{|V_{ts}|^2}{|V_{td}|^2} \tag{3.1}$$

One assumes here that the lifetime τ_b, the mass m_b, the B_B-parameter and the decay constant f_B, are all equal for B_d and B_s. In our parametrization

$$\frac{x_s}{x_d} = \frac{(s_{23})^2}{|s_{12}s_{23} - s_{13}e^{i\delta}|^2} = \frac{1}{|s_{12} - qe^{i\delta}|^2} \tag{3.2}$$

The ratio is a function of $q = \frac{s_{13}}{s_{23}}$ and δ only, and is independent of m_t and s_{23}. This ratio is minimized when δ is taken as close to 180° as possible (the phase δ cannot be exactly 180° because it would lead to $\epsilon = 0$):

$$\frac{x_s}{x_d} \geq \frac{1}{(s_{12} + q)^2} \geq 4.7 \tag{3.3}$$

where the second inequality results from $q \leq 0.22$. This gives:

$$x_s \geq 2.6 \Longrightarrow r_s \geq 0.77 \tag{3.4}$$

Thus, a large $B_s - \bar{B}_s$ mixing is expected, independently of m_t. Actually, for most of the range of the parameters we expect the mixing to be near-maximal.

With $\delta \sim 90^o$ we get $r_s \geq 0.94$. In fig. (11) we give lower limits on r_s for $0.02 \leq q \leq 0.22$, and $\delta \sim 90^o,\ 180^o$.

If q is negligible (compared to s_{12}) we expect $r_s = 0.985$.

3.2. DIRECT CP-VIOLATION: $\frac{\epsilon'}{\epsilon}$

The contribution from the "penguin" diagram to ϵ' gives [16]

$$\frac{\epsilon'}{\epsilon} \sim 6.0 C'' \left(\frac{s_{23} s_{13} \sin\delta}{s_{12}} \right) \tag{3.5}$$

where

$$C'' \equiv \left[\frac{Im\widetilde{C}_6}{-0.1} \right] \left[\frac{\langle \pi\pi | Q_6 | K^0 \rangle}{1.0\ GeV^3} \right] \tag{3.6}$$

The "penguin" operator is Q_6, while the Wilson coefficient is $\widetilde{C}_6$, where the CKM factor was explicitly taken out. The calculation of both $\widetilde{C}_6$ and $\langle \pi\pi | Q_6 | K^0 \rangle$ is subject to major theoretical ambiguities. The Wilson coefficient depends on the QCD scale and on m_t. As for the hadronic matrix element, recent lattice calculations [28] give values which are much smaller than the vacuum insertion approximation. In addition, one has to correct the C'' parameter for isospin breaking effects and for electromagnetic "penguin" graphs. On all of these ambiguities we have nothing to add here. Our analysis concerns only the product of the mixing angles and the phase.

The CKM factor is maximal for $s_{23} \sim 0.05$, $q \sim 0.22$ and δ close to 90^o. This would give $\epsilon'/\epsilon \sim 1.5 \times 10^{-2} C''$. A lower limit on the CKM factor is derived when q is at its lower limit ~ 0.02 (in which case $\sin\delta \sim O(1)$ from the ϵ-bound). We get $\epsilon'/\epsilon \sim 8 \times 10^{-4} C''$. This lower limit is determined by the ϵ bound, so at this stage the $B - \bar{B}$ mixing data do not improve the predictions. We will, however, return to the subject when we study the Fritzsch scheme in sect. (5.4).

The three recent experimental results are [29]:

$$\begin{aligned}\frac{\epsilon'}{\epsilon} &= (-0.46 \pm 0.53 \pm 0.24) \times 10^{-2} \\ \frac{\epsilon'}{\epsilon} &= (+0.17 \pm 0.82) \times 10^{-2} \\ \frac{\epsilon'}{\epsilon} &= (+0.35 \pm 0.30 \pm 0.20) \times 10^{-2}\end{aligned} \tag{3.7}$$

3.3. $K^+ \to \pi^+ \nu\bar{\nu}$

The branching ratio for the decay $K^+ \to \pi^+ \nu\bar{\nu}$ is [20]

$$BR(K^+ \to \pi^+ \nu\bar{\nu}) = 2\chi^2 BR(K^+ \to \pi^0 e^+ \nu_e) \sum_{i=1}^{3} \frac{\left|\sum_{j=2}^{3} V_{js}^* V_{jd} D(y_j, z_i)\right|^2}{|V_{us}|^2} \tag{3.8}$$

where $z_i = \frac{[m(\ell_i)]^2}{M_W^2}$ and

$$\begin{aligned}D(y,z) = &-\frac{1}{8}\frac{yz}{z-y}\left(\frac{4-z}{1-z}\right)^2 \ln(z) + \frac{1}{4}y + \frac{3}{8}\left(1 - \frac{3}{1-z}\right)\frac{y}{1-y} \\ &+\frac{1}{8}\left[\frac{y}{z-y}\left(\frac{4-y}{1-y}\right)^2 + 1 + \frac{3}{(1-y)^2}\right] y \ln(y)\end{aligned} \tag{3.9}$$

We use [30]

$$\begin{aligned}\chi &\equiv \frac{\alpha}{4\pi \sin^2 \theta_W} = 0.0025 \\ BR(K^+ &\to \pi^0 e^+ \nu_e) = 0.048\end{aligned} \tag{3.10}$$

and get [20]

$$BR(K^+ \to \pi^+ \nu\bar{\nu}) = 6.0 \times 10^{-7} \sum_i \hat{D}_i \tag{3.11}$$

where

$$\hat{D}_i \equiv \frac{\left|\sum_{j=2}^{3} V_{js}^* V_{jd} D(y_j, z_i)\right|^2}{|V_{us}|^2} = |D(y_c, z_i) + \frac{s_{23}}{s_{12}} V_{td} D(y_t, z_i)|^2 \tag{3.12}$$

The z_i can be put to zero, except for z_τ in $D(y_c, z_\tau)$, where the non-negligible

mass of the τ gives a smaller D:

$$D(y_c, z_e) = D(y_c, z_\mu) = 3.9 \times 10^{-3} \quad ; D(y_c, z_\tau) = 3.1 \times 10^{-3} \tag{3.13}$$

The second term in $\hat{D}_i$ depends on all three parameters (m_t, q, δ). The two terms in $\hat{D}_i$ give comparable contributions.

To get an *upper* limit on the branching ratio we replace (in eq. (3.12)) V_{td} with $|V_{td}|$ and put for s_{23} and $|V_{td}|$ their upper limits. An upper limit on $|V_{td}|$ is derived from the direct limits on s_{23} and s_{13}, $|V_{td}| \leq 0.022$. An indirect upper limit on $|V_{td}|$ is derived from the x_d relation (eq. (2.28)) with $x_d = 0.91$, $\tau_b = 1$ *psec* and $B_B f_B^2 = (0.1\ GeV)^2$. It is more stringent than the first limit only for $m_t \geq 140\ GeV$. The upper limit on the branching ratio is shown in fig. (12.a). It varies from 9×10^{-11} for $m_t = 45\ GeV$ to 5.3×10^{-10} for $m_t = 180\ GeV$.

A *lower* limit is derived by taking the lower limits of both $\frac{s_{23}}{s_{12}}|V_{td}|$ and $\frac{s_{23}}{s_{12}} Re(V_{td})$. We note that the lower limit on the real part can be considerably smaller than that on the absolute value. The lower limit on $|V_{td}|$ is derived from eq. (2.28) with $x_d = 0.55$, $\tau_b = 1.32$ *psec* and $B_B f_B^2 = (0.2\ GeV)^2$. As for $Re(V_{td})$, we numerically searched for the minimum in all the allowed range of the parameters (s_{23}, q, δ) and checked for consistency with the lower bound on $|V_{td}|$. The lower bound on the branching ratio is also shown in fig. (12.a) and is in the range $(6-7) \times 10^{-11}$.

The limits on $BR(K^+ \to \pi^+ \nu\bar{\nu})$ were previously studied in ref. [3]. The range of parameters used here and in ref. [3] is slightly different. When this difference is taken into account the upper limits agree, but our lower limit is lower by approximately a factor of 2.

For the central values of the parameters we find $BR(K^+ \to \pi^+ \nu\bar{\nu}) = (1.4 - 1.8) \times 10^{-10}$. The present experimental upper limit is [30]

$$BR(K^+ \to \pi^+ \nu\bar{\nu}) \leq 1.4 \times 10^{-7} \tag{3.14}$$

3.4. $K_L^0 \to \mu^+\mu^-$

The short distance contribution to the decay $K_L^0 \to \mu^+\mu^-$ is given by [20]

$$BR(K_L^0 \to \mu^+\mu^-)_{SD} = 4\chi^2 \frac{\tau(K_L^0)}{\tau(K^+)} BR(K^+ \to \mu^+\nu_\mu) \frac{\left[Re\sum_{j=2}^{3} V_{js}^* V_{jd} C(y_j)\right]^2}{|V_{us}|^2} \tag{3.15}$$

where

$$C(y) = \frac{3}{4}\left(\frac{y}{1-y}\right)^2 \ln(y) + \frac{1}{4}y + \frac{3}{4}\frac{y}{1-y} \tag{3.16}$$

In addition to the previous parameters we now use [30]

$$\begin{aligned} BR(K^+ \to \mu^+\nu_\mu) &= 0.64 \\ \tau(K_L) &= 5.2 \times 10^{-8} sec \\ \tau(K^+) &= 1.2 \times 10^{-8} sec \end{aligned} \tag{3.17}$$

We get

$$BR(K_L^0 \to \mu^+\mu^-)_{SD} = 6.7 \times 10^{-5} \hat{C} \tag{3.18}$$

where

$$\hat{C} \equiv \frac{\left[Re\sum_{j=2}^{3} V_{js}^* V_{jd} C(y_j)\right]^2}{|V_{us}|^2} = \left[C(y_c) + \frac{s_{23}}{s_{12}} Re(V_{td}) C(y_t)\right]^2 \tag{3.19}$$

We find $C(y_c) = 3.3 \times 10^{-4}$ and $C(y_t) = O(1)$ so, as in the case of $K \to \pi\nu\bar{\nu}$, the two terms in $\hat{C}$ are of the same order of magnitude.

We find the limits on the short distance contribution to the branching ratio in methods similar to those described in the previous section. The upper limit is shown in fig. (12.b). It varies from 2×10^{-10} for $m_t = 45\ GeV$ to 5.6×10^{-9} for

$m_t = 180\ GeV$. The experimental result is [30]

$$BR(K_L^0 \to \mu^+\mu^-) = (9.1 \pm 1.8) \times 10^{-9} \tag{3.20}$$

However, one usually assumes [31] that the important contribution to this mode comes not from the short distance diagrams but from the two-photon intermediate state. Subtracting the calculated two photon contribution gives [31] that the short distance contribution should be less than 5.6×10^{-9}. Even our upper limit is consistent with this bound. The central solutions of (m_t, q, δ) give $BR(K_L^0 \to \mu^+\mu^-)_{SD} = (4.8 - 13.5) \times 10^{-10}$, and a lower limit can be put of order 1×10^{-10}. These results indeed support the importance of the two photon intermediate state to this decay.

3.5. $b \to s\nu\bar{\nu}$

The branching ratio for the decay $b \to s\nu\bar{\nu}$ is given by [32]

$$BR(b \to s\nu\bar{\nu}) = \chi^2 BR(b \to (u,c)\ell\bar{\nu}_\ell) \sum_{i=1}^{3} \frac{\left|\sum_{j=2}^{3} V_{js}^* V_{jb} D(y_j, z_i)\right|^2}{|V_{ub}|^2 + F(m_c^2/m_b^2)|V_{cb}|^2} \tag{3.21}$$

Using

$$BR(b \to (u,c)\ell\bar{\nu}_\ell) = 0.12 \tag{3.22}$$

we get

$$BR(b \to s\nu\bar{\nu}) = 7.5 \times 10^{-7} \cdot 3\hat{D}_B \tag{3.23}$$

where

$$\hat{D}_B \equiv \frac{\left|\sum_{j=2}^{3} V_{js}^* V_{jb} D(y_j, z=0)\right|^2}{|V_{ub}|^2 + F(m_c^2/m_b^2)|V_{cb}|^2} = \frac{[D(y_t,0) - D(y_c,0)]^2}{q^2 + F(m_c^2/m_b^2)} \approx \frac{[D(y_t,0)]^2}{F(m_c^2/m_b^2)} \tag{3.24}$$

As the contribution of the c-quark is very small, the effect of putting $m_\tau \to 0$ is negligible. The branching ratio is, to a good approximation, a function of m_t

only. This is shown in fig. (12.c). The branching ratio varies from 2×10^{-6} for $m_t = 45\ GeV$ to 4.6×10^{-5} for $m_t = 180\ GeV$.

The quark level decay discussed here may be realized in the hadronic level by $B \to K\nu\bar{\nu}$, or by more complicated final hadronic states such as $K\pi$, $K\pi\pi$ etc.

3.6. $b \to s\gamma$

The branching ratio for the decay $b \to s\gamma$ is given by [33]

$$BR(b \to s\gamma) = \frac{3\alpha}{2\pi} BR(b \to (u,c)\ell\bar{\nu}_\ell) \frac{\left|\sum_{j=2}^{3} V_{js}^* V_{jb} F_2(y_j)\right|^2}{|V_{ub}|^2 + F(m_c^2/m_b^2)|V_{cb}|^2} \tag{3.25}$$

where

$$F_2(y) = \left[\frac{2}{3(y-1)} + \frac{7}{4(y-1)^2} + \frac{1}{2(y-1)^3}\right] y + \frac{y^2(1-\frac{3}{2}y)}{(y-1)^4} \ln(y) \tag{3.26}$$

Using the known parameters we get

$$BR(b \to s\gamma) = 4.5 \times 10^{-4} \hat{F} \tag{3.27}$$

where

$$\hat{F} \equiv \frac{\left|\sum_{j=2}^{3} V_{js}^* V_{jb} F_2(y_j)\right|^2}{|V_{ub}|^2 + F(m_c^2/m_b^2)|V_{cb}|^2} = \frac{[F_2(y_t) - F_2(y_c)]^2}{q^2 + F(m_c^2/m_b^2)} \approx \frac{[F_2(y_t)]^2}{F(m_c^2/m_b^2)} \tag{3.28}$$

In the last approximation we used $F_2(y_c) = 1.9 \times 10^{-4} \ll F_2(y_t) = O(10^{-1})$. For $m_t < M_W$ one cannot ignore QCD corrections. The main effect is to replace [34]

$$F_2(y_t) \to [F_2(y_t) + \frac{4}{3}\frac{\alpha_s}{\pi} \ln(y_t/y_B)] \tag{3.29}$$

where $y_B = M_B^2/M_W^2$. The QCD correction always dominates the $F_2(y_t)$ term.

Again, we are in a situation where the branching ratio depends on m_t only. This is shown in fig. (12.d). The dashed line shows the results with the QCD correction. This calculation becomes unreliable when m_t approaches M_W. The branching ratio varies from 1×10^{-5} (8×10^{-5} with QCD corrections) for $m_t = 45\ GeV$ to 1.3×10^{-4} for $m_t = 180\ GeV$. The quark level process $b \to s\gamma$ is realized in the hadronic decays $B \to K^{(i)}\gamma$, where $K^{(i)}$ are excited states of the kaon. The decay into the ground state K^0 is forbidden by angular momentum considerations. The calculation of the exclusive modes involves further hadronic uncertainties [35].

In conclusion, we analyzed the implications of the parameters (m_t, q, δ) on several experimental measurements. The r_s and ϵ'/ϵ values are determined by q and δ, and are independent of m_t. The rare B decays, are determined by m_t and insensitive to q values. The rare K decays are functions of all three parameters.

4. Relations among masses and angles

4.1. SCHEMES FOR MASS MATRICES

Within the standard model, the quark sector is described by ten free parameters. In the *physical* (mass) basis, these are the six quark masses, three mixing angles and one phase. These parameters can all be experimentally determined. Whatever their experimental values are, the standard model remains self-consistent.

In the *interaction* basis, our parameters are entries of the yet undiagonalized mass matrices. If we had some theoretical principle from which we could determine the mass matrices, we would predict the values of the physical parameters. In several schemes of mass matrices, the number of independent entries of the mass matrices is less than ten: either some entries vanish or there are relations among the non-vanishing entries. These schemes provide us with relations among quark masses, angles and phases (the motivation for such relations is discussed, for example, in ref. [36]).

One should check that these relations are consistent with the experimental data. If the relations suggested by a certain scheme are not compatible with the experimental constraints, then either the scheme is incorrect, or the use of its predictions should await the finding of additional new physics.

We discuss four schemes for mass matrices: the Fritzsch scheme [7], the Fritzsch scheme with the Shin phases [9], the Stech scheme [8] and the Gronau - Johnson - Schechter (GJS) scheme [10]. These schemes were consistent with all previous data [7 – 10, 37, 38]. We check in chapters 5 and 6 their consistency with the new $B - \bar{B}$ mixing measurement (combined with earlier data).

4.2. EXPLICIT FORMS OF MASS MATRICES

The Fritzsch scheme suggests that in the interaction basis the quark mass matrices are of the form

$$M^q = \begin{pmatrix} 0 & a^q e^{i\phi_a} & 0 \\ a^q e^{i\phi'_a} & 0 & b^q e^{i\phi_b} \\ 0 & b^q e^{i\phi'_b} & c^q e^{i\phi_c} \end{pmatrix} \tag{4.1}$$

By a redefinition of the phases of the right-handed up quarks and of the right-handed down quarks we can bring both M^u and M^d to a hermitian form. By further rotating both left-handed and right-handed (up and down) quarks with the *same* unitary phase-matrix, we can make M^u real. Thus, without loss of generality, we can choose a basis [39, 38] in which the Fritzsch matrices have the form:

$$M^u = \begin{pmatrix} 0 & a^u & 0 \\ a^u & 0 & b^u \\ 0 & b^u & c^u \end{pmatrix} \quad M^d = \begin{pmatrix} 0 & a^d e^{i\phi_1} & 0 \\ a^d e^{-i\phi_1} & 0 & b^d e^{i\phi_2} \\ 0 & b^d e^{-i\phi_2} & c^d \end{pmatrix} \tag{4.2}$$

Within the Fritzsch scheme, the quark sector is described by eight parameters. Therefore we expect this scheme to provide us with *two* predictions for relations among quark masses, angles and phases.

Within the Fritzsch scheme, Shin suggested the following ansatz for the phases [9]:

$$|\phi_1| = 90^o \;\; ; \;\; |\phi_2| = 0^o \tag{4.3}$$

The motivation for such values is that they may naturally arise in certain types of Higgs potentials. The Fritzsch scheme with the phases fixed has only six independent parameters. Thus we now have *four* predictions for relations among the quark sector parameters.

The Stech scheme suggests that in the interaction basis the quark mass matrices have the following properties:

$$\begin{aligned} M^u &= M^{u\dagger} = M^{uT} \\ M^d &= M^{d\dagger} = \alpha M^u + A \end{aligned} \tag{4.4}$$

where A is an antisymmetric matrix and α is a constant. Actually, the mass matrices need not be hermitian, but can always be brought to a hermitian form without affecting the low energy parameters. As M^u is a real symmetric matrix it can be brought to a diagonal form by an orthogonal transformation. In this new basis the mass matrices are of the form [8]

$$M^u = \begin{pmatrix} m_u & 0 & 0 \\ 0 & -m_c & 0 \\ 0 & 0 & m_t \end{pmatrix} \; ; \; M^d = \begin{pmatrix} \alpha m_u & ia & ib \\ -ia & -\alpha m_c & ic \\ -ib & -ic & \alpha m_t \end{pmatrix} \tag{4.5}$$

The a, b and c parameters are all real. Within the Stech scheme, the quark sector is described by seven parameters. It gives us *three* relations among quark masses, mixing angles and phases.

Gronau, Johnson and Schechter [10] suggested to have mass matrices of the Fritzsch form (4.2), with the Stech constraints (4.4). This scheme has only six independent parameters, leading to *four* predictions of relations among quark masses, mixing angles and phases.

4.3. QUARK MASSES

The masses of the quarks, which are the eigenvalues of the mass matrices to be discussed, are not the *physical* masses but parameters in the Lagrangian. This means that they are *running* masses, which should all be taken at a single energy scale. In the different schemes, the three mixing angles and the phase depend on *mass ratios* rather than on the masses themselves. As mass ratios are, to a good approximation, independent of the energy scale, the scale itself can be arbitrarily chosen. Following ref. [40] we use:

$$\begin{aligned} m_d/m_s &= 0.051 \pm 0.004 \\ m_u/m_c &= 0.0038 \pm 0.0012 \\ m_s/m_b &= 0.033 \pm 0.011 \end{aligned} \tag{4.6}$$

In our calculations we ignore the relatively small error on m_d/m_s, but we consider the full range of the other ratios.

The relations we get involve the undetermined mass ratio m_c/m_t. In order to confront these relations with the x_d and ϵ bounds, involving the physical mass of the t quark m_t^{phys}, we must:

a. Specify m_c at a certain energy scale μ. We take $\mu = 1\ GeV$. The value of $m_c(\mu = 1\ GeV)$ is given in ref. [40]:

$$m_c(\mu = 1\ GeV) = 1.35 \pm 0.05\ GeV \tag{4.7}$$

b. Translate the relations involving m_c/m_t into relations that depend on the running top mass $m_t(\mu = 1\ GeV)$.

c. Write these relations in terms of the physical mass of the t quark. The relation between the physical mass and the running mass, including a first

order QCD correction, is [40]:

$$m_t^{phys} = m_t(\mu = m_t)\left[1 + \frac{4}{3\pi}\alpha_s(m_t)\right]. \tag{4.8}$$

In order to relate $m_t(\mu = m_t)$ to $m_t(\mu = 1\ GeV)$ we use the usual equation for the running mass [40]:

$$m(\mu) = \bar{m}\cdot\left(1 - \frac{2\beta_1\gamma_0}{\beta_0^3}\frac{\ln L + 1}{L} + \frac{8\gamma_1}{\beta_0^2 L}\right)\left(\frac{L}{2}\right)^{-2\gamma_0/\beta_0} \tag{4.9}$$

where:

$$\begin{aligned} \beta_0 &= 11 - \frac{2}{3}N_f\ ;\ \gamma_0 = 2 \\ \beta_1 &= 102 - \frac{38}{3}N_f\ ;\ \gamma_1 = \frac{101}{12} - \frac{5}{18}N_f \\ L &= \ln(\mu^2/\Lambda^2)\ ;\ \Lambda = 0.1\ GeV \end{aligned} \tag{4.10}$$

and $\bar{m}$ is the renormalization group invariant mass. The physical mass of the top quark as a function of its running mass at 1 GeV is given in fig. (13). A good approximation for m_t^{phys} in the interesting range between 40 GeV and 180 GeV is $m_t^{phys} \sim 0.6\ m_t(\mu = 1\ GeV)$ (we use the full expression in our calculations). In what follows we, again, denote the physical mass of the t quark by m_t.

5. The Fritzsch scheme for quark masses

5.1. THE EIGHT PARAMETERS

We study mass matrices of the form

$$M^u = \begin{pmatrix} 0 & a^u & 0 \\ a^u & 0 & b^u \\ 0 & b^u & c^u \end{pmatrix} \quad M^d = \begin{pmatrix} 0 & a^d e^{i\phi_1} & 0 \\ a^d e^{-i\phi_1} & 0 & b^d e^{i\phi_2} \\ 0 & b^d e^{-i\phi_2} & c^d \end{pmatrix} \tag{5.1}$$

The six real parameters $(a^u, b^u, c^u, a^d, b^d, c^d)$ can be expressed in terms of the six

quark masses:

$$\begin{aligned} a^u &\approx \sqrt{m_u m_c}\ ;\ b^u \approx \sqrt{m_c m_t}\ ;\ c^u \approx m_t \\ a^d &\approx \sqrt{m_d m_s}\ ;\ b^d \approx \sqrt{m_s m_b}\ ;\ c^d \approx m_b \end{aligned} \tag{5.2}$$

The approximation is good to $O(m_d/m_s) \sim (1/20)$. The two phases (ϕ_1, ϕ_2) can be expressed in terms of the quarks masses and the two *known* mixing angles, s_{12} and s_{23}

$$s_{12} \approx \left| \sqrt{\frac{m_d}{m_s}} - e^{-i\phi_1} \sqrt{\frac{m_u}{m_c}} \right| \tag{5.3}$$

$$s_{23} \approx \left| \sqrt{\frac{m_s}{m_b}} - e^{-i\phi_2} \sqrt{\frac{m_c}{m_t}} \right| \tag{5.4}$$

Thus, all eight parameters of the Fritzsch scheme are expressible in terms of seven known parameters (five quark masses and two mixing angles) and the yet unknown mass of the top quark. Consequently, for every selected value of m_t, we get predictions for the unknown mixing angle, s_{13}:

$$s_{13} \approx \left| \frac{m_s}{m_b} \sqrt{\frac{m_d}{m_b}} + e^{-i\phi_1} \sqrt{\frac{m_u}{m_c}} \left(\sqrt{\frac{m_s}{m_b}} - e^{-i\phi_2} \sqrt{\frac{m_c}{m_t}} \right) \right| \tag{5.5}$$

and for the phase δ [38]:

$$\frac{\sin\delta}{\frac{s_{12}s_{23}}{s_{13}} - \cos\delta} \approx \frac{\sin\phi_1}{\cos\phi_1 - \sqrt{\frac{m_d m_c}{m_s m_u}}} \tag{5.6}$$

In this chapter we find whether the predictions (5.5) and (5.6) are consistent with the allowed ranges obtained in chapter 2.

5.2. SIMPLE LIMITS ON THE RANGE OF PARAMETERS

Eq. (5.4) gives a lower limit on the unknown mass ratio $\frac{m_c}{m_t}$:

$$\frac{m_c}{m_t} \geq \left(\sqrt{\frac{m_s}{m_b}} - s_{23}\right)^2 \tag{5.7}$$

Using $\frac{m_s}{m_b} \geq 0.022$ and $s_{23} \leq 0.050$ we get

$$\frac{m_c}{m_t} \geq 0.01 \Longrightarrow m_t(\mu = 1\ GeV) \leq 145\ GeV \tag{5.8}$$

For other values of m_s/m_b and s_{23} we get more stringent bounds. For example, the central values $m_s/m_b = 0.033$ and $s_{23} = 0.043$ give $m_t(\mu = 1\ GeV) \leq 73\ GeV$.

We find that the bound (5.8) is translated into a bound on the physical mass $m_t \leq 88\ GeV$, so we study the predictions of the Fritzsch scheme only for

$$43\ GeV \leq m_t \leq 88\ GeV. \tag{5.9}$$

The lower limit is the one derived from the ϵ and x_d bounds in chapter 2. As mentioned above, other values of m_s/m_b and s_{23} lead to more stringent bounds. The upper bound corresponding to central values, $m_t(\mu = 1\ GeV) \leq 73\ GeV$, leads to a bound on the physical mass $m_t \leq 47\ GeV$.

Eq. (5.9) considerably reduces the range of parameters that we need to study. It is possible to further reduce this range without exact calculations by considering eq. (5.5). First, we rewrite eq. (5.5) in the following way:

$$q = \frac{s_{13}}{s_{23}} = \left|\frac{1}{s_{23}}\left(\frac{m_s}{m_b}\right)^{3/2}\sqrt{\frac{m_d}{m_s}} + e^{-i(\phi_1+\phi_3)}\sqrt{\frac{m_u}{m_c}}\right| \tag{5.10}$$

The phase ϕ_3 is defined through $s_{23}e^{-i\phi_3} \equiv \sqrt{\frac{m_s}{m_b}} - e^{-i\phi_2}\sqrt{\frac{m_c}{m_t}}$. This gives an

upper limit on q:

$$q \leq \frac{1}{s_{23}} \left(\frac{m_s}{m_b}\right)^{3/2} \sqrt{\frac{m_d}{m_s}} + \sqrt{\frac{m_u}{m_c}} \tag{5.11}$$

Using $m_s/m_b \leq 0.044$, $m_u/m_c \leq 0.005$ and $s_{23} \geq 0.034$ we get $q \leq 0.13$, so we study the predictions of the Fritzsch scheme only for

$$0.02 \leq q \leq 0.13 \tag{5.12}$$

The lower bound is the one derived from the ϵ and x_d bounds. For other values of m_s/m_b and s_{23} we get more stringent bounds. For example, the central values $m_s/m_b = 0.033$ and $s_{23} = 0.043$ give $q \leq 0.10$.

In fig. (6) we gave the allowed region in the $m_t - q$ plane. The two bounds (5.9) and (5.12) overlap within this allowed region only for

$$\begin{aligned} 56\ GeV \leq & m_t \leq 88\ GeV \\ 0.04 \leq & q \leq 0.13 \end{aligned} \tag{5.13}$$

Thus, in order to check consistency of the Fritzsch scheme with the allowed (m_t, q, δ) values, we need to make explicit calculations only within the bounds (5.13).

5.3. RESULTS

We calculated the values of q and δ predicted by eqs. (5.10) and (5.6). This was done as follows:

a. We select a value for m_u/m_c and find ϕ_1 from eq. (5.3). We note that the sign of ϕ_1 is undetermined.

b. We select values for m_s/m_b, m_c/m_t and s_{23} and find ϕ_2 from eq. (5.4). Again, the sign of ϕ_2 is undetermined.

c. We find q from eq. (5.10). The two possible relative signs between ϕ_1 and ϕ_2 give two possible solutions.

d. We find δ by solving eq. (5.6). For each of the two solutions of q, there are two possible solutions for δ corresponding to the two possible signs of ϕ_1.

Thus, for each selected set of parameters s_{23}, m_c/m_t, m_s/m_b and m_u/m_c we have several possible solutions for q and δ.

On the other hand, for each set of values of m_t and s_{23} we have an allowed region for q and δ from the experimental measurements (as given, for example, in fig. (4)). We then check whether the Fritzsch predictions are within the allowed range.

We find that for almost all values of the parameters the Fritzsch solutions are below the experimental lower bounds. In order to get a consistent solution

a. The mass ratio m_s/m_b should be close to its lower limit, $m_s/m_b \sim 0.022$.

b. The mixing angle s_{23} should be close to its upper limit, $s_{23} \sim 0.050$.

c. The $B-\bar{B}$ mixing parameter x_d should be close to its lower limit, $x_d \sim 0.55$.

d. The B decay constant f_B should be close to the upper limit of its theoretical evaluation, $B_B f_B^2 \sim (0.20\ GeV)^2$.

e. The B_K constant should be close to the upper limit of its theoretical evaluation, $B_K \sim 1$.

Only if all of these conditions are simultaneously fulfilled, there is a very narrow region of (m_t, q, δ) which is consistent with both the Fritzsch relations and the experimental data. This region is within the following bounds:

$$\begin{aligned} 82\ GeV \leq & m_t \leq 88\ GeV \\ 0.06 \leq & q \leq 0.08 \\ 96^o \leq & \delta \leq 110^o \end{aligned} \tag{5.14}$$

In fig. (14) we show the Fritzsch solutions consistent with the experimental data for $m_t = 85\ GeV$ and for $q = 0.07$.

We remind the reader that when we gave the ϵ and the x_d bounds we did not add errors in quadrature but allowed for the full range of all parameters. The consistency of the Fritzsch scheme and the three generation standard model requires many experimental and theoretical quantities to simultaneously assume values at the limits of their allowed ranges. This is an unlikely situation. However, the Fritzsch scheme cannot be completely excluded.

In conclusion, if the Fritzsch scheme is to be consistent with the standard model, then the three unknown parameters of the quark sector should assume the values

$$m_t \sim 85\ GeV\ ;\ q \sim 0.07\ ;\ \delta \sim 100^o. \tag{5.15}$$

The bounds on other known parameters of the quark sector become more stringent,

$$s_{23} \sim 0.05\ ;\ m_s/m_b \sim 0.22. \tag{5.16}$$

The values of s_{23} and q give $s_{13} \sim 0.0035$. In addition, there are no ambiguities in the ϵ-relation ($B_K \sim 1$) and in the x_d-relation ($x_d \sim 0.55$, $B_B f_B^2 \sim (0.2\ GeV)^2$).

5.4. PREDICTIONS

The Fritzsch scheme provided us with a full determination of all the parameters of the quark sector in the three generation standard model. Thus, it predicts the results of future experiments which depend on these parameters. We now give the predictions for all the experiments described in chapter 3. We use the values given in eqs. (5.15) and (5.16).

(1) The x_s-parameter assumes the value (eq. (3.2)):

$$x_s \approx \frac{x_d}{(s_{12})^2} = 11 \Longrightarrow r_s = 0.98 \tag{5.17}$$

Thus $B_s - \bar{B}_s$ mixing is near maximal.

(2) For the CP-violating parameter ϵ'/ϵ we get (eq. (3.5)):

$$\frac{\epsilon'}{\epsilon} \sim 0.47 \times 10^{-2} C'' \tag{5.18}$$

If $C'' \sim 1$, this is close to the level studied by present experiments.

(3) The calculation of the rare kaon decays is simplified by taking $y_t = \frac{m_t^2}{M_W^2} \approx 1$. In the expression (3.8) for $BR(K^+ \to \pi^+ \nu\bar{\nu})$ we have $D(y_t = 1, z = 0) = \frac{11}{8}$. Consequently $\hat{D}_e = \hat{D}_\mu = 5.7 \times 10^{-5}$ and $\hat{D}_\tau = 4.6 \times 10^{-5}$. This gives

$$BR(K^+ \to \pi^+ \nu\bar{\nu}) = 6.0 \times 10^{-7} \sum_i \hat{D}_i = 9.6 \times 10^{-11} \tag{5.19}$$

(4) For the $K_L^0 \to \mu^+\mu^-$ decay (eq. (3.15)), we have $C(y_t = 1) = \frac{5}{8} \to \hat{C} = 4.0 \times 10^{-6}$, and consequently

$$BR(K_L^0 \to \mu^+\mu^-)_{SD} = 6.7 \times 10^{-5} \hat{C} = 2.7 \times 10^{-10}, \tag{5.20}$$

which is consistent with the assumption that the two-photon intermediate state dominates this mode.

We note that as $m_t \approx M_W$, QCD corrections to the above calculations are small and may be neglected.

(5) In the calculation of the rare B decays we again put $y_t \approx 1$. As discussed before, the other parameters do not affect the results, because we normalize our results to the semi-leptonic branching ratio. For the $b \to s\nu\bar{\nu}$ mode (eq. (3.23)), we have $\hat{D}_B = \frac{2.0}{F(m_c^2/m_b^2)}$ and consequently

$$BR(b \to s\nu\bar{\nu}) = 7.5 \times 10^{-7} \cdot 3\hat{D}_B = 8.7 \times 10^{-6} \tag{5.21}$$

(6) For the radiative decay (eq. (3.25)) we have $F_2(y_t = 1) = \frac{5}{24}$. As $m_t \sim M_W$

we ignore the QCD corrections. We get

$$BR(b \to s\gamma) = 4.5 \times 10^{-4} \hat{F} = 4 \times 10^{-5} \tag{5.22}$$

QCD corrections are likely to give a somewhat higher value for this branching ratio.

(7) We note that the low value of $s_{13} \sim 0.035$ predicted by the Fritzsch scheme indicates that non-charmed B-decays will not be observed in the near future. In particular

$$0.006 \leq \frac{\Gamma(b \to u\ell\bar{\nu}_\ell)}{\Gamma(b \to c\ell\bar{\nu}_\ell)} \leq 0.015 \tag{5.23}$$

where we have used the full range of q (eq. (5.14)) and $F(m_c^2/m_b^2)$ (eq. (2.11)). If there is a direct observation of such a mode in the near future, it is likely to give a lower bound on $q = \frac{s_{13}}{s_{23}}$ which is higher than the upper bound of the Fritzsch scheme, $q \leq 0.08$. Thus, such an observation may exclude the Fritzsch scheme. As for non-leptonic non-charmed decays, the calculation of their branching ratios is subject to large uncertainties. Using the calculations and the parameters presented in ref. [41], we find

$$\begin{aligned}
BR(\bar{B}^0 \to \pi^+\pi^-) &\sim 1 \times 10^{-5} \\
BR(\bar{B}^0 \to \pi^+\rho^-) &\sim 3 \times 10^{-5} \\
BR(\bar{B}^0 \to \pi^+ A_1^-) &\sim 3 \times 10^{-5} \\
BR(\bar{B}^0 \to \rho^+\rho^-) &\sim 2 \times 10^{-5} \\
BR(\bar{B}^0 \to \rho^+ A_1^-) &\sim 3 \times 10^{-5}
\end{aligned} \tag{5.24}$$

5.5. THE FRITZSCH SCHEME WITH THE SHIN PHASES

In our calculations of the Fritzsch scheme parameters we find $|\phi_1| \sim 78^o$ and $|\phi_2| \sim 6^o$. The proximity of these phases to the Shin ansatz, $|\phi_1| = 90^o$ and $|\phi_2| = 0^o$, makes it interesting to check whether this ansatz can be accomodated with the experimental data.

The values of the six real parameters are the same as in the general Fritzsch scheme (eq. (5.2)).

The mixing angle s_{12} is given by

$$s_{12} \approx \left(\frac{m_d}{m_s} + \frac{m_u}{m_c}\right)^{1/2} \tag{5.25}$$

As all three parameters in this equation are known, we should check this relation for consistency. We find that it suggests that both mass ratios should be close to their lower limits, $\frac{m_d}{m_s} \sim 0.047$ and $\frac{m_u}{m_c} \sim 0.0026$, while the mixing angle is at its upper limit, $s_{12} \sim 0.222$.

The relation for s_{23}

$$s_{23} \approx \sqrt{\frac{m_s}{m_b}} - \sqrt{\frac{m_c}{m_t}}, \tag{5.26}$$

becomes a prediction for $\frac{m_c}{m_t}$: actually the lower limit in eq. (5.7) now becomes an equality. As we know already that the Fritzsch scheme is consistent with the experimental data only for $s_{23} \sim 0.05$, $\frac{m_s}{m_b} \sim 0.022$, we find

$$m_t(\mu = 1\ GeV) \sim 145\ GeV \Longrightarrow m_t \sim 88\ GeV. \tag{5.27}$$

As for the unknown mixing angle, s_{13} we get

$$q = \frac{s_{13}}{s_{23}} \approx \left[\frac{1}{(s_{23})^2}\left(\frac{m_s}{m_b}\right)^3 \frac{m_d}{m_s} + \frac{m_u}{m_c}\right]^{1/2} = 0.053 \tag{5.28}$$

For the phase δ we have

$$\frac{\sin\delta}{\frac{s_{12}}{q}-\cos\delta}\approx\sqrt{\frac{m_s m_u}{m_d m_c}}\Longrightarrow\delta=92^o \tag{5.29}$$

The allowed region for $q-\delta$ with $m_t=88\ GeV$ is shown in fig. (15). The Shin solution lies outside of the allowed region. It is consistent with the ϵ-bound but not with the x_d-bound. However, it lies very close to the allowed region, and as we ignored corrections of $O(\frac{m_s}{m_d})$ to the Fritzsch predictions we conclude that the Shin ansatz is still not completely ruled out. If we have an experimental lower bound on the ratio q in the near future, it may invalidate the Fritzsch matrices with the Shin phases.

6. The Stech scheme for quark masses

6.1. RELATIONS AMONG ANGLES AND MASSES

We study mass matrices of the form

$$M^u=\begin{pmatrix} m_u & 0 & 0\\ 0 & -m_c & 0\\ 0 & 0 & m_t\end{pmatrix}\ ;\ M^d=\begin{pmatrix} \alpha m_u & ia & ib\\ -ia & -\alpha m_c & ic\\ -ib & -ic & \alpha m_t\end{pmatrix} \tag{6.1}$$

The relations are most easily obtained [8] from

$$VM^{d(diag)}V^\dagger=\alpha M^{u(diag)}+\hat{A} \tag{6.2}$$

The matrix V is the CKM-mixing matrix (eq. (2.2)). The matrix $\hat{A}$ is hermitian and without diagonal elements, but in general it is not antisymmetric.

Equating the (3,3) element of both sides in eq. (6.2) gives $\alpha\approx\frac{m_b}{m_t}$.

Comparing the (1,1) element gives

$$m_d - (s_{12})^2 m_s + (s_{13})^2 m_b = \alpha m_u \Longrightarrow s_{12} \approx \sqrt{\frac{m_d}{m_s}} \tag{6.3}$$

which is consistent with the known values of s_{12} and $\frac{m_d}{m_s}$.

Comparing the (2,2) element gives

$$(s_{12})^2 m_d - m_s + (s_{23})^2 m_b = -\alpha m_c \Longrightarrow s_{23} \approx \sqrt{\frac{m_s}{m_b} - \frac{m_c}{m_t}} \tag{6.4}$$

The third relation is derived by noting [8] that the matrix $\hat{A}$, being hermitian and with no diagonal elements, fulfills $Re[\det \hat{A}] = 0$:

$$\begin{aligned} &Re[(-s_{12}m_s + s_{23}s_{13}e^{i\delta}m_b)(s_{12}s_{23}m_s + s_{13}e^{-i\delta}m_b)(s_{23}m_b)] = 0 \Longrightarrow \\ &\cos\delta \approx -\frac{m_s}{m_b}\frac{s_{12}}{q} + \frac{m_b}{m_s}\frac{(s_{23})^2 q}{s_{12}} \end{aligned} \tag{6.5}$$

6.2. RESULTS

For any given values of s_{23} and $\frac{m_s}{m_b}$ we have a prediction for $\frac{m_c}{m_t}$ (eq. (6.4)). This is translated into a value for $m_t(\mu = 1\ GeV)$ and then into the physical m_t in the manner described in sect. 4.3. An upper limit on m_t is obtained when $s_{23} = 0.050$, $\frac{m_s}{m_b} = 0.022$:

$$m_t(\mu = 1\ GeV) \leq 72\ GeV \Longrightarrow m_t \leq 46\ GeV. \tag{6.6}$$

As the experimental data gave $m_t \geq 43\ GeV$, there is only a very small "window" open for the Stech scheme:

$$43\ GeV \leq m_t \leq 46\ GeV \tag{6.7}$$

Lower values of s_{23} and higher values of $\frac{m_s}{m_b}$ give smaller m_t and are excluded by the experimental data.

For m_t as low as 45 GeV, the CKM-matrix element V_{td} should be near its upper limit in order to give large enough $B - \bar{B}$ mixing (see eqs. (2.26) and (2.27)). This requires $q \cos\delta \sim -0.20$ which, given the known values of s_{12} and $\frac{m_s}{m_b}$, is clearly inconsistent with the prediction (6.5). In fig (16) we show the region allowed for $q - \delta$ with $m_t \sim 45\ GeV$. We also show the curve representing the Stech scheme (eq. (6.5)). There is no overlap between the Stech prediction and the region allowed by experimental data. Thus we conclude: *Within a three generation standard model, the Stech scheme is excluded.*

6.3. THE GRONAU-JOHNSON-SCHECHTER SCHEME

The parameters in the GJS scheme obey all the constraints of both the Fritzsch scheme and the Stech scheme. Consequently, if any of these schemes is excluded, so is the GJS scheme. Thus we conclude that the GJS form of mass matrices is ruled out together with the Stech form.

7. Conclusions

We studied the quark sector parameters within the three generation standard model. We analyzed the constraints coming from two types of measurements: direct constraints from tree level decay widths, and indirect constraints from ϵ and x_d measurements. We find that the new $B - \bar{B}$ mixing data, when combined with the CP-violation data, give the following *new* bound:

$$m_t \geq 43\ GeV \tag{7.1}$$

In addition, for any given value of m_t we found the allowed region for s_{13}/s_{23} and δ. Alternatively, for any given value of s_{13}/s_{23} we give the allowed region of m_t and δ.

The new constraints allow us to improve the predictions of future experimental results. The $B_s - \bar{B}_s$ mixing is expected to be near maximal. The ratio

ϵ'/ϵ can be at the level of present experiments, but much smaller values are still possible. We get the following bounds on rare decays branching ratios:

$$\begin{aligned} 5 \times 10^{-11} &\leq BR(K^+ \to \pi^+ \nu\bar{\nu}) \leq 5.4 \times 10^{-10} \\ 9 \times 10^{-11} &\leq BR(K_L^0 \to \mu^+\mu^-)_{SD} \leq 5.6 \times 10^{-9} \\ 2 \times 10^{-6} &\leq BR(b \to s\nu\bar{\nu}) \leq 4.6 \times 10^{-5} \\ 1 \times 10^{-5} &\leq BR(b \to s\gamma) \leq 1.3 \times 10^{-4} \end{aligned} \tag{7.2}$$

Different schemes for quark mass matrices give additional relations among quark masses, mixing angles and phases. Thus, the range of parameters is further constrained. We find that the Fritzsch scheme is inconsistent with the experimental data for most of the range of the different parameters. Only if many parameters simultaneously assume values near their experimental or theoretical bounds: $B_K \sim 1$, $B_B f_B^2 \sim (0.2\ GeV)^2$, $x_d \sim 0.55$, $s_{23} \sim 0.05$ and $m_s/m_b \sim 0.022$, we get a very small allowed region of parameters near the values:

$$m_t \sim 85\ GeV\ ;\ s_{13} \sim 0.0035\ ;\ \delta \sim 100^o \tag{7.3}$$

As all parameters are practically determined by this unique solution, it gives very definite predictions for all the experiments mentioned above:

$$\begin{aligned} & r_s \sim 0.98 \\ & \frac{\epsilon'}{\epsilon} \sim 0.47 \times 10^{-2} C'' \\ & BR(K^+ \to \pi^+ \nu\bar{\nu}) \sim 9.6 \times 10^{-11} \\ & BR(K_L^0 \to \mu^+\mu^-)_{SD} \sim 2.7 \times 10^{-10} \\ & BR(b \to s\nu\bar{\nu}) \sim 8.7 \times 10^{-6} \\ & BR(b \to s\gamma) \sim 4 \times 10^{-5} \\ & \frac{\Gamma(b \to u\ell\bar{\nu}_\ell)}{\Gamma(b \to c\ell\bar{\nu}_\ell)} \sim 0.01 \end{aligned} \tag{7.4}$$

The Fritzsch solution with the Shin phases is more unlikely to be consistent with the experimental data but it is not completely ruled out.

The Stech form is excluded by the new data. Even when all parameters are taken to their extreme values, the Stech relations cannot be fulfilled within the allowed range of parameters. The GJS extension of the Stech scheme is also ruled out.

All our bounds and conclusions are valid within the three generation standard model. They remain valid in theories beyond the standard model provided that there are no significant contributions to CP violation and to $B-\bar{B}$ mixing from processes other than those present in the standard model (see ref. [6] for recent studies of $B-\bar{B}$ mixing in theories beyond the standard model). Our results cannot be applied if a fourth generation exists.

We gave here improved constraints on the three parameters m_t, q and δ. Two of these, m_t and $q = s_{13}/s_{23}$, may soon be *directly* measured. If m_t is found to be less than 40 GeV, new physics beyond the three generation standard model is implied. The prediction that r_s is near maximal is valid in the standard model as well as in many extensions of it. If we find $r_s \leq 0.77$, the most likely possibility is the existence of a fourth generation.

Many near future experiments may rule out the Fritzsch scheme. A direct observation of non charmed b decays (implying $q > 0.08$) is the most reasonable candidate to do that. If we find $m_t < 82\ GeV$ or $r_s < 0.98$ the Fritzsch scheme will be excluded. If we find better ways to calculate s_{23} and get $s_{23} < 0.05$, again the Fritzsch scheme will not be valid. However, if this better calculation gives an upper bound which is weaker than the one we use (or if experiments find a shorter b lifetime than is quoted now), the constraints on the Fritzsch scheme may be loosened up a little.

We expect the accumulation of new data from B physics to provide us with a much better knowledge of the standard model parameters. We should be able to decide whether a three generation standard model still gives a satisfactory picture of the experimental data and whether the Fritzsch scheme is consistent with this picture.

I thank Ikaros Bigi and Fred Gilman for valuable discussions. I am especially grateful to Haim Harari for his advice and help. I acknowledge the support of a Fulbright fellowship.

REFERENCES

1. U. Amaldi et al., University of Pennsylvania preprint, UPR-0331T (1987)
2. ARGUS Collaboration, DESY preprint 87-029 (1987)
3. J. Ellis, J.S. Hagelin and S. Rudaz, CERN preprint, CERN-TH.4679/87 (1987)
4. I.I. Bigi and A.I. Sanda, SLAC preprint, SLAC-PUB-4299 (1987);
   L.L. Chau and W.Y. Keung, UC Davis preprint, UCD-87-02 (1987);
   V. Barger, T. Han, D.V. Nanopoulos and R.J.N. Phillips, University of Wisconsin preprint, MAD/PH/341 (1987);
   D. Du and Z. Zhao, Princeton preprint, IASSNS-HEP-87/23 (1987);
   J. Maalampi and M. Roos, University of Helsinki preprint, HU-TFT-87-12 (1987)
5. H. Harari and Y. Nir, SLAC preprint, SLAC-PUB-4341 (1987), Phys. Lett. B, in print
6. G. Altarelli and P.J. Franzini, CERN preprint, CERN-TH.4745/87 (1987);
   W.S. Hou and A. Soni, University of Pittsburgh preprint, PITT-87-06 (1987);
   A. Datta, E.A. Paschos and U. Türke, University of Dortmund preprint, DO-TH-87/9 (1987)
7. H. Fritzsch, Phys. Lett. 70B (1977) 436; Phys. Lett. 73B (1978) 317
8. B. Stech, Phys. Lett. 130B (1983) 189
9. M. Shin, Phys. Lett. 145B (1984) 285
10. M. Gronau, R. Johnson and J. Schechter, Phys. Rev. Lett. 54 (1985) 2176
11. L. Maiani, Phys. Lett. 62B (1976) 183;
    L. Wolfenstein, Phys. Rev. Lett. 51 (1984) 1945;
    L.L. Chau and W.Y. Keung, Phys. Rev. Lett. 53 (1984) 1802

12. H. Harari and M. Leurer, Phys. Lett. 181B (1986) 123

13. W.J. Marciano and A. Sirlin, BNL preprint, BNL-39658 (1987)

14. J.S. Hagelin, Nucl. Phys. B193 (1981) 123

15. G. Altarelli et al., Nucl. Phys. B208 (1982) 365;
B. Grinstein, M.B. Wise and N. Isgur, Phys. Rev. Lett. 56 (1986) 298

16. F.J. Gilman and J.S. Hagelin, Phys. Lett. 133B (1983) 443

17. E.H. Thorndike, *in* Proc. of the 1985 International Symposium on Lepton and Photon Interactions at High Energies, eds. M. Konuma and K. Takahashi, (Kyoto, 1985)

18. M.G.D. Gilchriese, Cornell preprint, CLNS-86/754 (1986)

19. CLEO collaboration, Cornell preprint, CLNS 87/78 (1987)

20. T. Inami and C.S. Lim, Prog. Theo. Phys. 65 (1981) 297; (E) 65 (1981) 1772

21. F.J. Gilman and M.B. Wise, Phys. Rev. D27 (1983) 1128

22. A.J. Buras, W. Slominski and H. Steger, Nucl. Phys. B238 (1984) 529; B245 (1984) 369

23. L.J. Reinders, H. Rubinstein and S. Yazaki, Phys. Rep. 127 (1985) 1

24. T.M. Aliev and V.L. Eletskii, Sov. J. Nucl. Phys. 38 (1983) 936

25. M. Suzuki, Phys. Lett. 162B (1985) 392

26. E. Golowich, Phys. Lett. 91B (1980) 271

27. H. Krasemann, Phys. Lett. 96B (1980) 397;
S. Godfrey, Phys. Rev. D33 (1986) 1391

28. S.R. Sharpe et al., SLAC preprint, SLAC-PUB-4236 (1987)

29. R.H. Bernstein et al., Phys. Rev. Lett. 54 (1985) 1631;
J.K. Black et al., Phys. Rev. Lett. 54 (1985) 1628;
B. Winstein, invited talk at the Division of Particles and Fields Meeting, Salt Lake City, Utah, Jan. 1987

30. Particle Data Group, Phys. Lett. 170B (1986) 1

31. R.E. Shrock and M.B. Voloshin, Phys. Lett. 87B (1979) 375;
J. Ellis and J.S. Hagelin, Nucl. Phys. B217 (1983) 189

32. W.S. Hou, R.S. Willey and A. Soni, Phys. Rev. Lett. 58 (1987) 1608

33. B.A. Campbell and P.J. O'Donnell, Phys. Rev. D25 (1982) 1989;
P.J. O'Donnell, Phys. Lett. 175B (1986) 369;
W.S. Hou, A. Soni and H. Steger, University of Pittsburgh preprint, PITT-87-01 (1987)

34. S. Bertolini, F. Borzumati and A. Masiero, Carnegie Mellon preprint, CMU-HEP 86-19 (1986)

35. N.G. Deshpande, P. Lo, J. Trampetic, G. Eilam and P. Singer, University of Oregon preprint, OITS-346 (1986);
T. Altomari, Carnegie Mellon preprint, CMU-HEP 87-08 (1987)

36. H. Harari, *in* Proc. of the 14th SLAC Summer Institute on Particle Physics, ed. E.C. Brennan (SLAC, 1986)

37. M. Shin, Harvard preprint HUTP-84/A070;
H. Fritzsch, Phys. Lett. 166B (1986) 423

38. M. Leurer, Weizmann Institute Ph.D. thesis, 1985, unpublished

39. H. Georgi and D.V. Nanopoulos, Nucl. Phys. B155 (1979) 52;
H. Fritzsch, Nucl. Phys. B155 (1979) 189;
L.F. Li, Phys. Lett. 84B (1979) 461

40. J. Gasser and H. Leutwyler, Phys. Rep. 87 (1982) 77

41. M. Bauer, B. Stech and M. Wirbel, Z. Phys. C34 (1987) 103

FIGURE CAPTIONS

Figure 1: Examples of the ϵ bounds. (a) Allowed range of $q = \frac{s_{13}}{s_{23}}$ and δ for $m_t = 55,\ 120\ GeV$ and $B_K = 1$. Heavy and light solid lines give, respectively, the central value and the edges of the band allowed by ϵ. The dotted line is the direct upper limit on q. The shaded area is the allowed region. (b) Allowed range of m_t and δ for $q = 0.20,\ 0.06$ and $B_K = 1$. Heavy and light solid lines give, respectively, the central value and the edges of the band allowed by ϵ. The dotted lines are the direct limits on m_t. The shaded area is the allowed region.

Figure 2: Examples of the x_d bounds. (a) Allowed range of $q = \frac{s_{13}}{s_{23}}$ and δ for $m_t = 55,\ 120\ GeV$. Heavy and light dashed lines give, respectively, the central value and the edges of the band allowed by x_d. For $m_t = 55\ GeV$ the upper bound is outside the graph. The dotted line is the direct upper limit on q. The shaded area is the allowed region. (b) Allowed range of m_t and δ for $q = 0.20,\ 0.06$. Heavy and light dashed lines give, respectively, the central value and the edges of the band allowed by x_d. For $q = 0.06$ the upper bound is outside of the graph. The dotted lines are the direct limits on m_t. The shaded area is the allowed region.

Figure 3: (a) Allowed range of $q = \frac{s_{13}}{s_{23}}$ and δ for $m_t = 55,\ 120\ GeV$ and $B_K = 1$. The meaning of the lines are as in figs. (1.a) and (2.a). The central solution (the intersection point of the two central curves) is denoted by a solid circle. For $m_t = 55\ GeV$ the central solution lies outside of the direct bounds. The shaded area is the final allowed region. (b) Allowed range of m_t and δ for $q = 0.20,\ 0.06$ and $B_K = 1$. The meaning of the lines are as in figs. (1.b) and (2.b). The central solution is denoted by a solid circle. The shaded area is the final allowed region.

Figure 4: Allowed range and central solutions of $q = \frac{s_{13}}{s_{23}}$ and δ for $m_t = 45,\ 65,\ 85,\ 180\ GeV$ and $B_K = 1$. Solid lines give the ϵ bounds. Dashed lines give the x_d bounds. The dotted line gives the direct bound. The

central solution is denoted by a solid circle. The shaded area is the final allowed region.

Figure 5: Allowed range of $q = \frac{s_{13}}{s_{23}}$ and δ for $m_t = 45,\ 65,\ 85,\ 180\ GeV$ and $B_K = 0.7$. The meaning of the lines, the solid circle and the shaded area are as in fig. (4).

Figure 6: Allowed range of $q = \frac{s_{13}}{s_{23}}$ and δ for $m_t = 45,\ 65,\ 85,\ 180\ GeV$ and $B_K = 0.4$. The meaning of the lines, the solid circle and the shaded area are as in fig. (4). There is no allowed region for $m_t = 45\ GeV$.

Figure 7: Allowed range of m_t and δ for $q = 0.18,\ 0.14\ 0.10,\ 0.04$ and $B_K = 1$. Solid lines give the ϵ bounds. Dashed lines give the x_d bounds. Dotted lines give the direct bounds on m_t. The central solution is denoted by a solid circle. The shaded area is the final allowed region.

Figure 8: Allowed range of m_t and δ for $q = 0.18,\ 0.14\ 0.10,\ 0.04$ and $B_K = 0.7$. The meaning of the lines, the solid circle and the shaded area are as in fig. (7).

Figure 9: Allowed range of m_t and δ for $q = 0.18,\ 0.14\ 0.10,\ 0.04$ and $B_K = 0.4$. The meaning of the lines, the solid circle and the shaded area are as in fig. (7). For $q = 0.04$ there is no allowed region.

Figure 10: Allowed range (shaded) of q and m_t for $B_K = 1,\ 0.7,\ 0.4$ and the curve (dot-dash) representing the central values. Dotted lines represent direct bounds while the solid curve is the indirect bound from the combination of the ϵ and the x_d bounds.

Figure 11: Lower limits on r_s for $\delta \sim 180^o$ (solid line) and $\delta \sim 90^o$ (dotted line) as a function of $q = \frac{s_{13}}{s_{23}}$.

Figure 12: (a) Upper and lower limits on $BR(K^+ \to \pi^+ \nu\bar{\nu})$ as a function of m_t. (b) The upper limit on the short distance contribution to $BR(K_L^0 \to \mu^+\mu^-)$ as a function of m_t (solid line). The dotted line gives the experimental value for this branching ratio. The dot-dashed line gives

the calculated upper limit on the short distance contribution. (c) The branching ratio $BR(b \to s\nu\bar{\nu})$ as a function of m_t. (d) The branching ratio $BR(b \to s\gamma)$ as a function of m_t. The solid line gives the results without QCD corrections. The dashed line includes QCD corrections, with the assumption $m_t \ll M_W$.

Figure 13: The physical mass of the t quark m_t^{phys} as a function of the running mass at 1 GeV, $m_t(\mu = 1\ GeV)$.

Figure 14: (a) Allowed range of q and δ for $m_t = 85\ GeV$, $B_K \leq 1$. The small shaded area is the overlap of the region allowed by the Fritzsch scheme and the region allowed by the data. Higher m_t values are excluded by the Fritzsch predictions. For lower m_t values there is no overlap between the two allowed regions. Solid, dashed and dotted lines are defined as in fig. (4). (b) Allowed range of m_t and δ for $q = 0.07$, $B_K \leq 1$. The small shaded area is the overlap of the region allowed by the Fritzsch scheme and the region allowed by the data. For other values of q there is no overlap between the two allowed regions. Solid, dashed and dotted lines are defined as in fig. (7).

Figure 15: Allowed range of q and δ for $m_t = 88\ GeV$, $B_K \leq 1$. The solid circle gives the Shin prediction. Higher m_t values are excluded by the Shin predictions. For lower m_t values the Shin solution lies even further out of the allowed region. Solid, dashed and dotted lines and the shaded area are defined as in fig. (4).

Figure 16: Allowed range (shaded) of q and δ for $m_t = 45\ GeV$, $B_K \leq 1$ and the curve (dot-dash) representing the Stech scheme. The two do not overlap. Higher m_t values are excluded by the Stech scheme. Lower m_t values are excluded by the data. Solid, dashed and dotted lines are defined as in fig. (4).

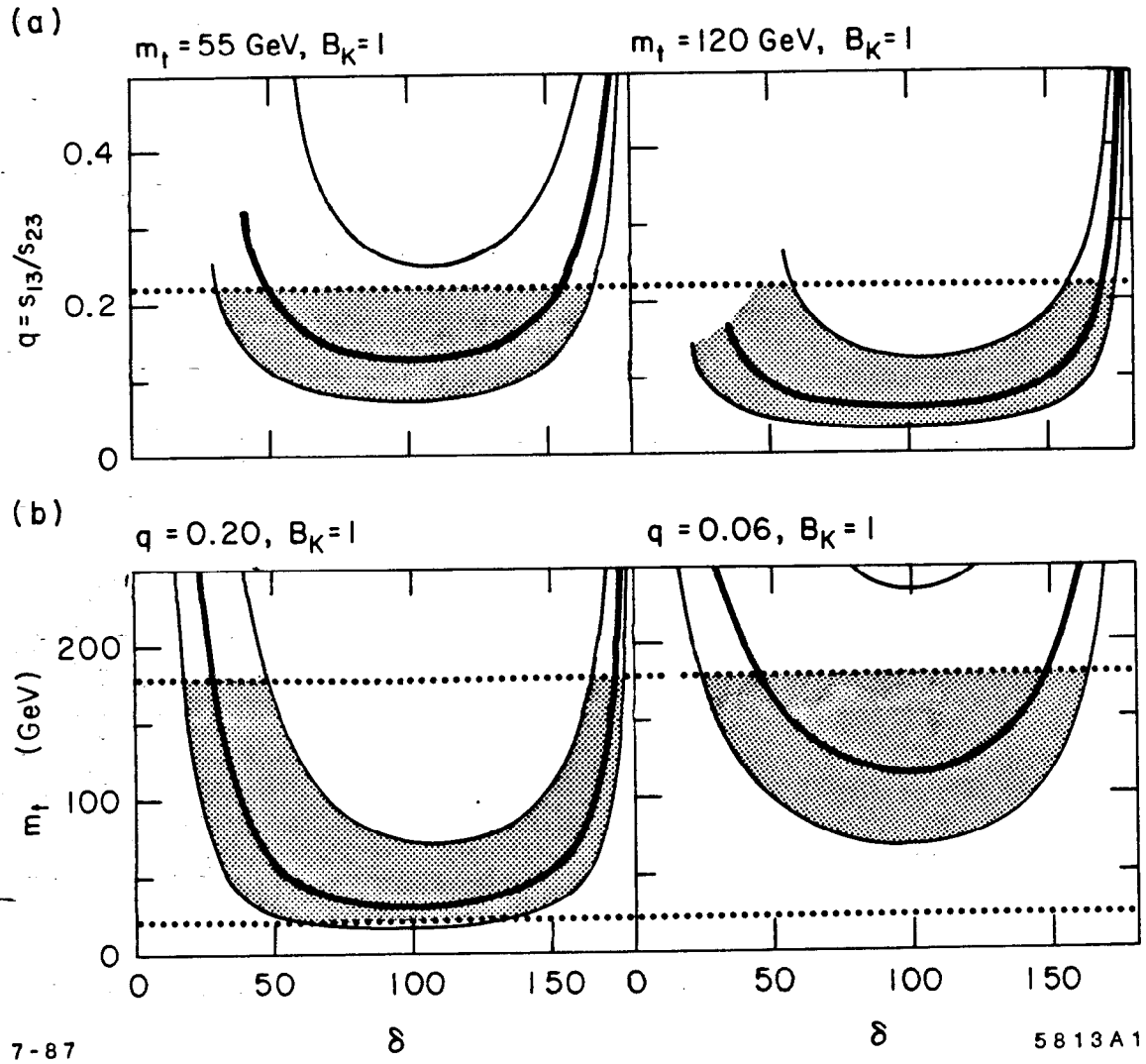
(a)
m_t = 55 GeV, B_K = 1
m_t = 120 GeV, B_K = 1
0.4
0.2
0
$q = s_{13}/s_{23}$
(b)
q = 0.20, B_K = 1
q = 0.06, B_K = 1
200
100
0
m_t (GeV)
0
50
100
150
δ
7-87
5813A1

Fig. 1

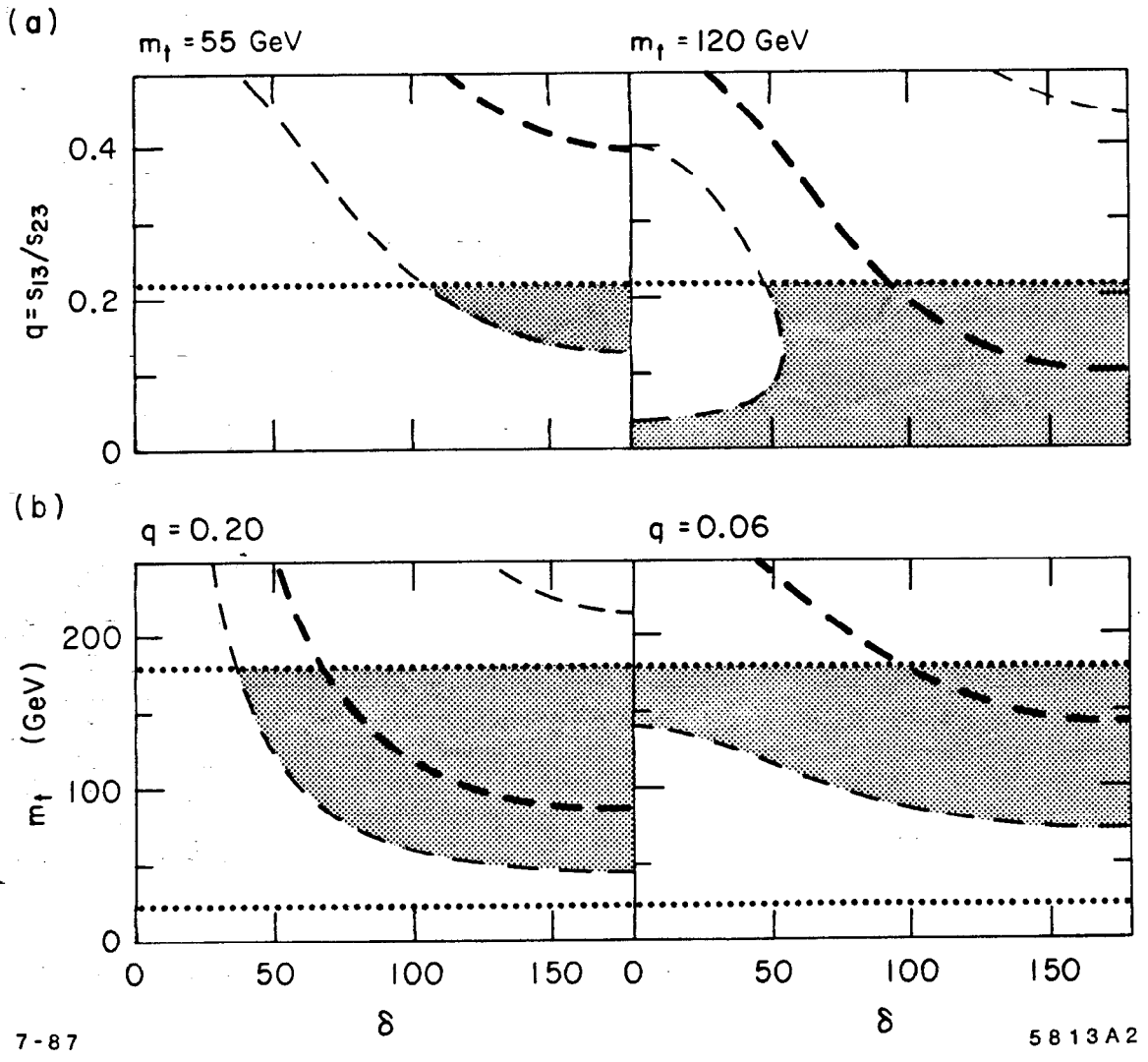
(a)
m_t = 55 GeV
m_t = 120 GeV
$q = s_{13}/s_{23}$
0.4
0.2
0
(b)
q = 0.20
q = 0.06
m_t (GeV)
200
100
0
0
50
100
150
δ
7-87
5813A2

Fig. 2

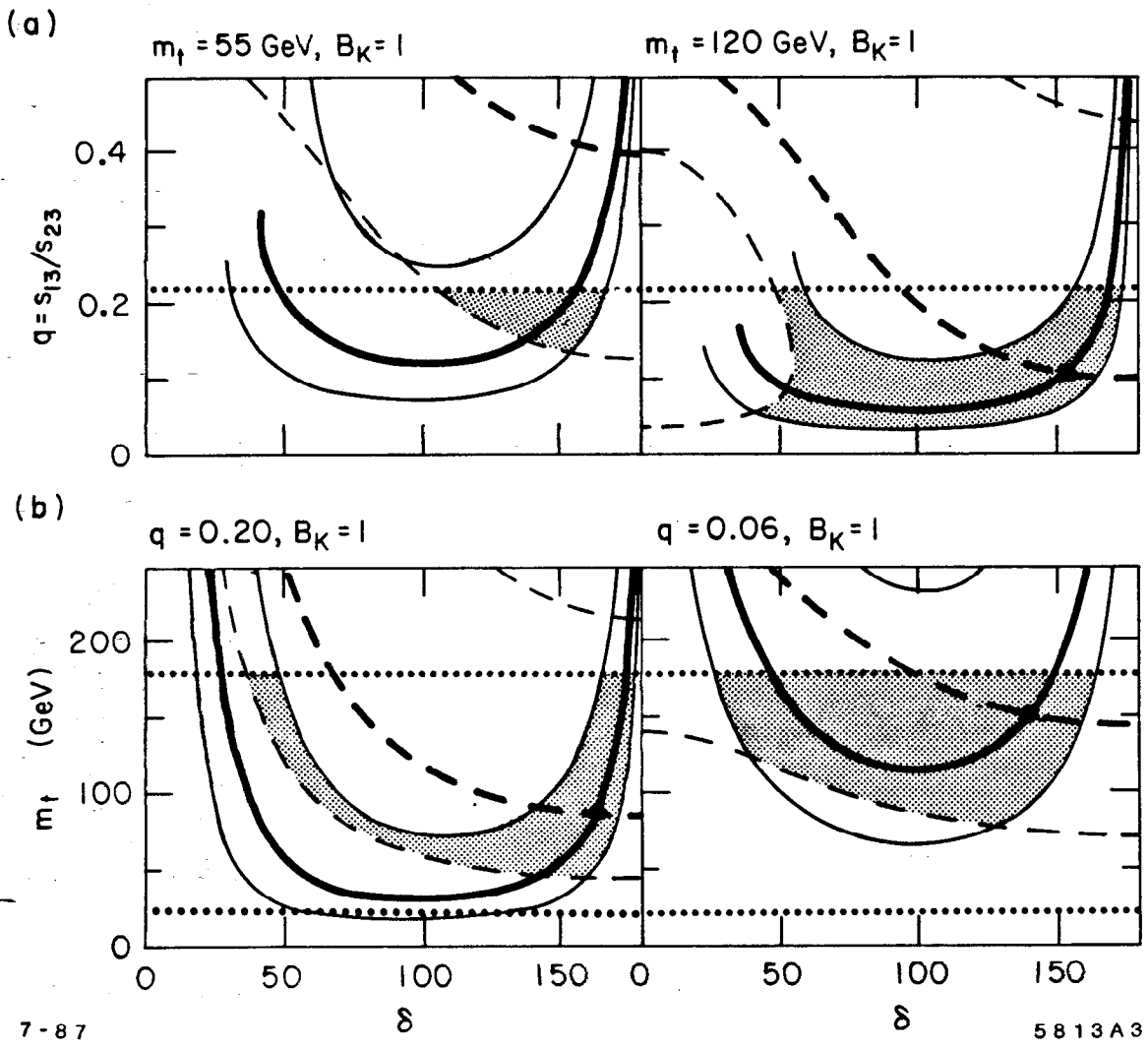
(a)
m_t = 55 GeV, B_K = 1
m_t = 120 GeV, B_K = 1
0.4
0.2
0
$q = s_{13}/s_{23}$
(b)
q = 0.20, B_K = 1
q = 0.06, B_K = 1
200
100
0
m_t (GeV)
0
50
100
150
δ
7-87
5813A3

Fig 3

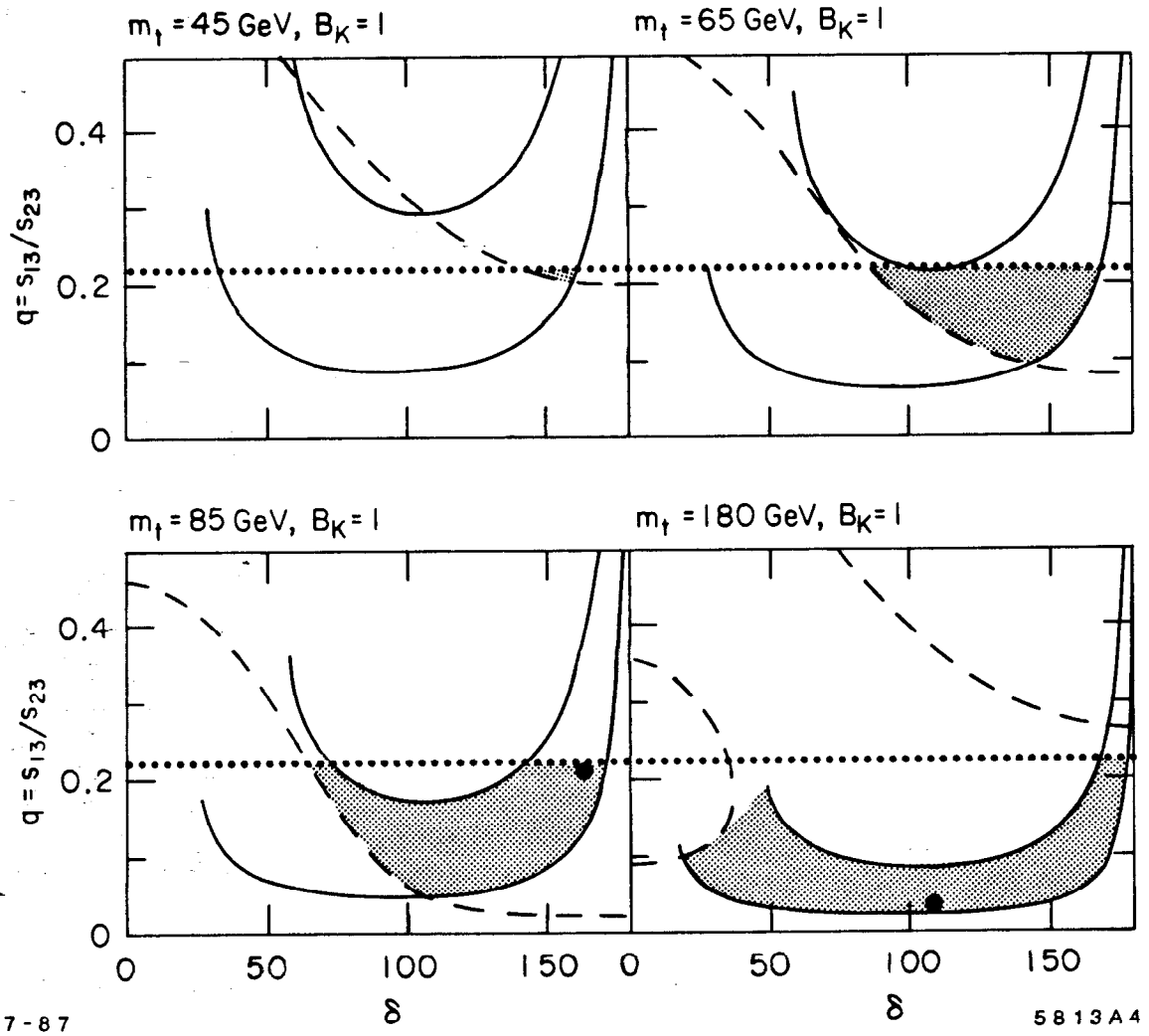
m_t = 45 GeV, B_K = 1
m_t = 65 GeV, B_K = 1
m_t = 85 GeV, B_K = 1
m_t = 180 GeV, B_K = 1
$q = s_{13}/s_{23}$
0.4
0.2
0
0
50
100
150
δ
7-87
5813A4

Fig. 4

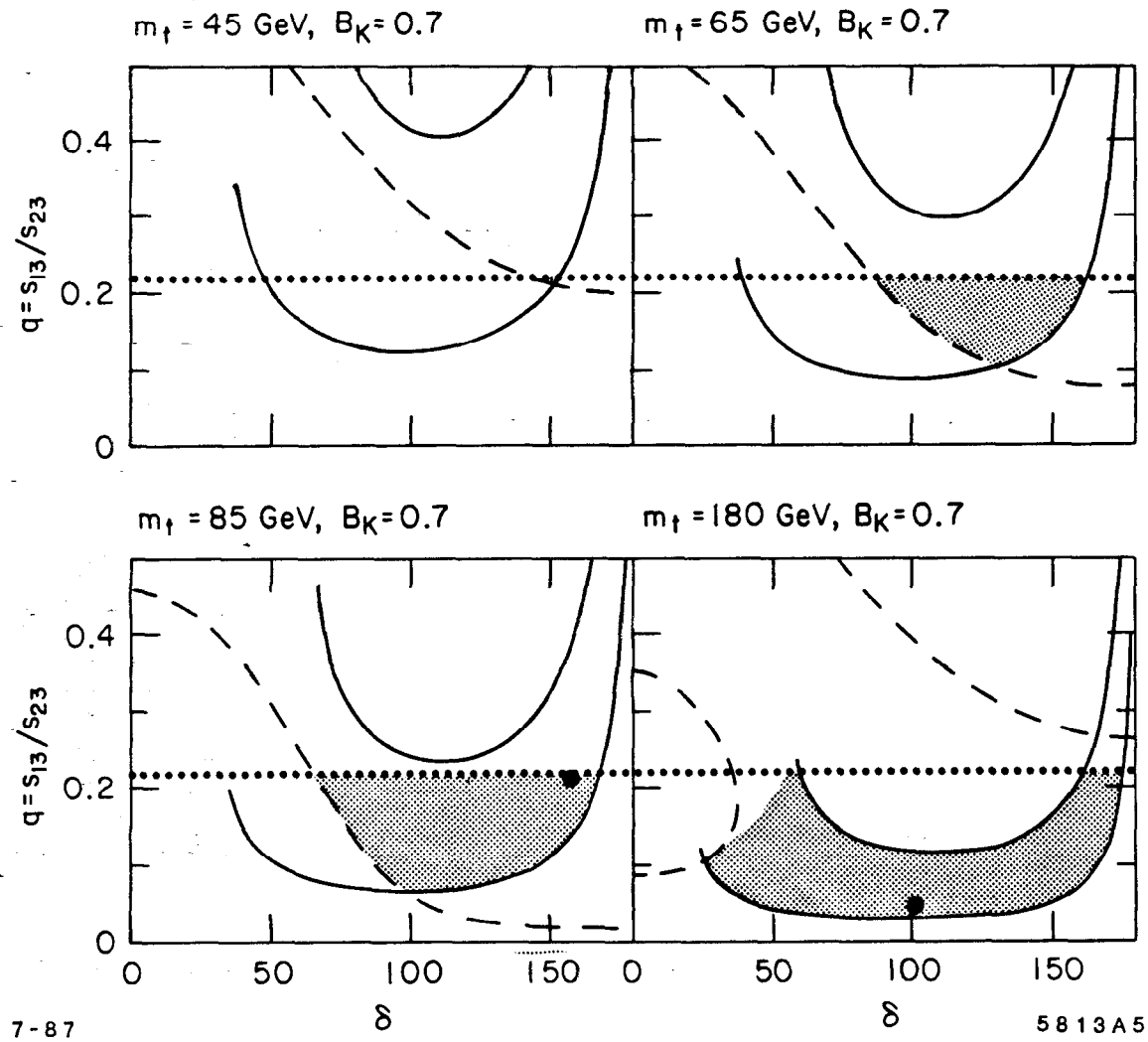
m_t = 45 GeV, B_K = 0.7
m_t = 65 GeV, B_K = 0.7
m_t = 85 GeV, B_K = 0.7
m_t = 180 GeV, B_K = 0.7
$q = s_{13}/s_{23}$
0.4
0.2
0
0
50
100
150
δ
7-87
5813A5

Fig 5

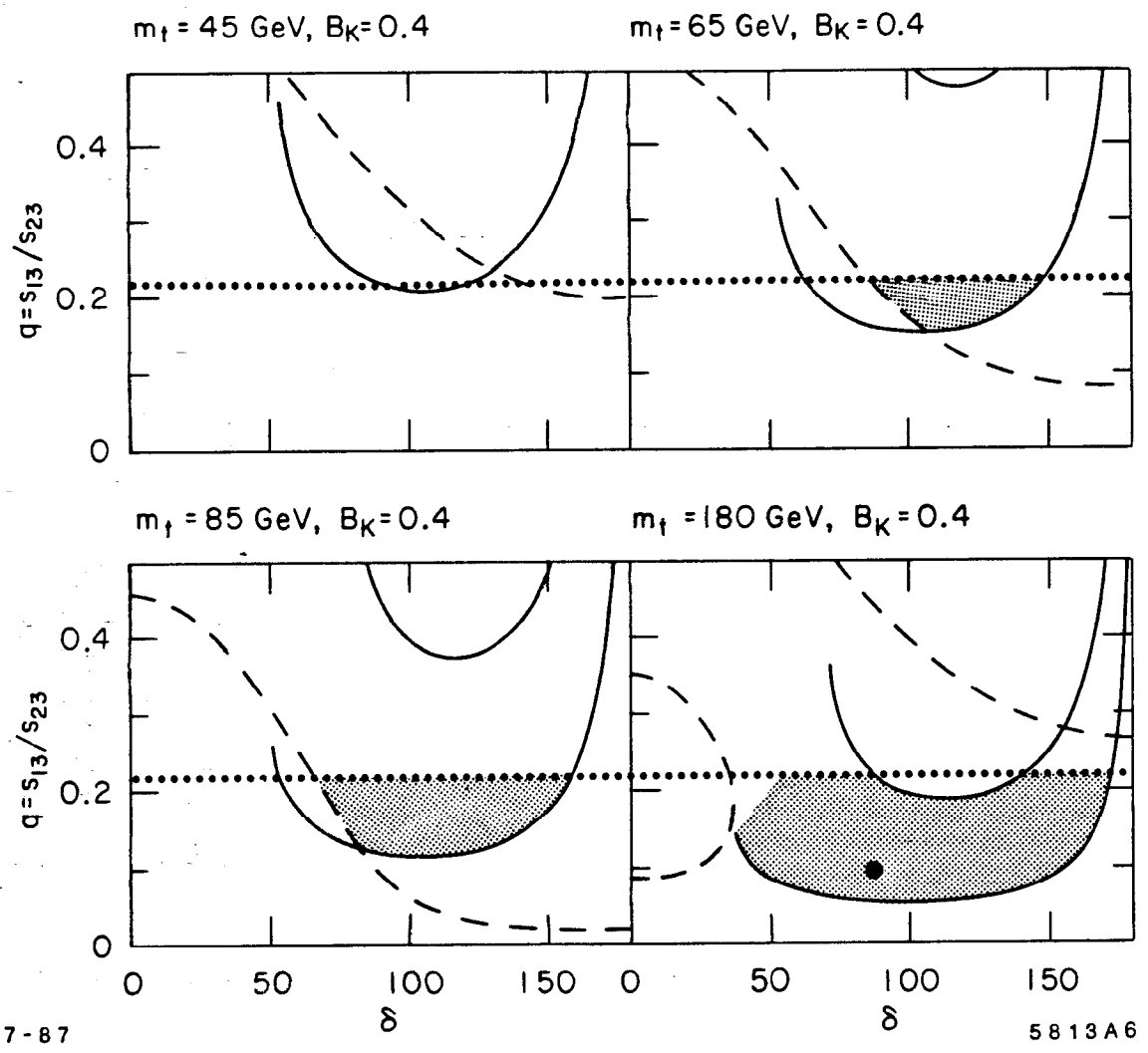
m_t = 45 GeV, B_K= 0.4
m_t = 65 GeV, B_K = 0.4
m_t = 85 GeV, B_K= 0.4
m_t = 180 GeV, B_K = 0.4
$q = s_{13}/s_{23}$
0.4
0.2
0
0
50
100
150
δ
7-87
5813A6

Fig. 6

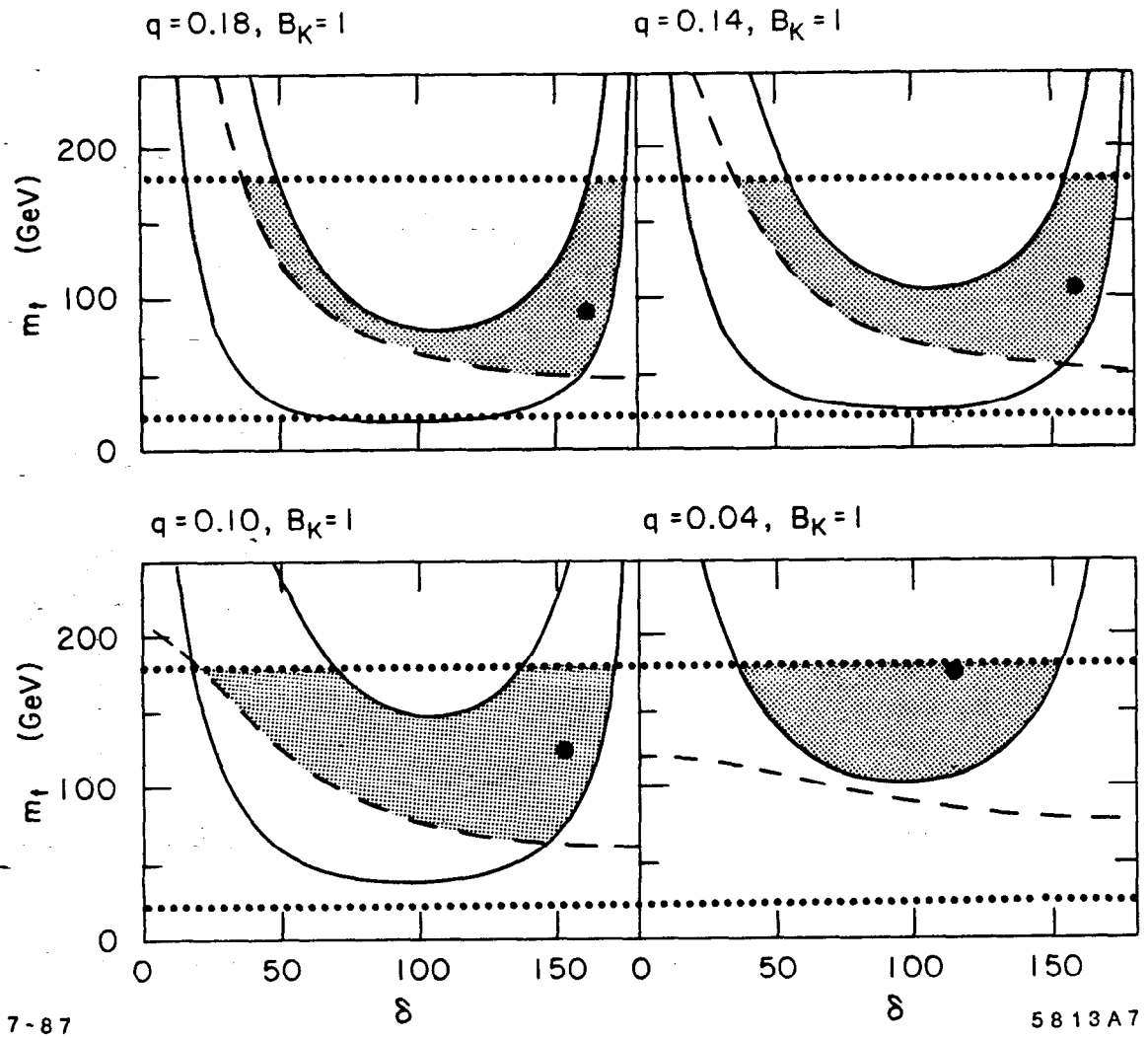
q = 0.18, B_K = 1
q = 0.14, B_K = 1
q = 0.10, B_K = 1
q = 0.04, B_K = 1
m_t (GeV)
200
100
0
0
50
100
150
δ
7-87
5813A7

Fig. 7

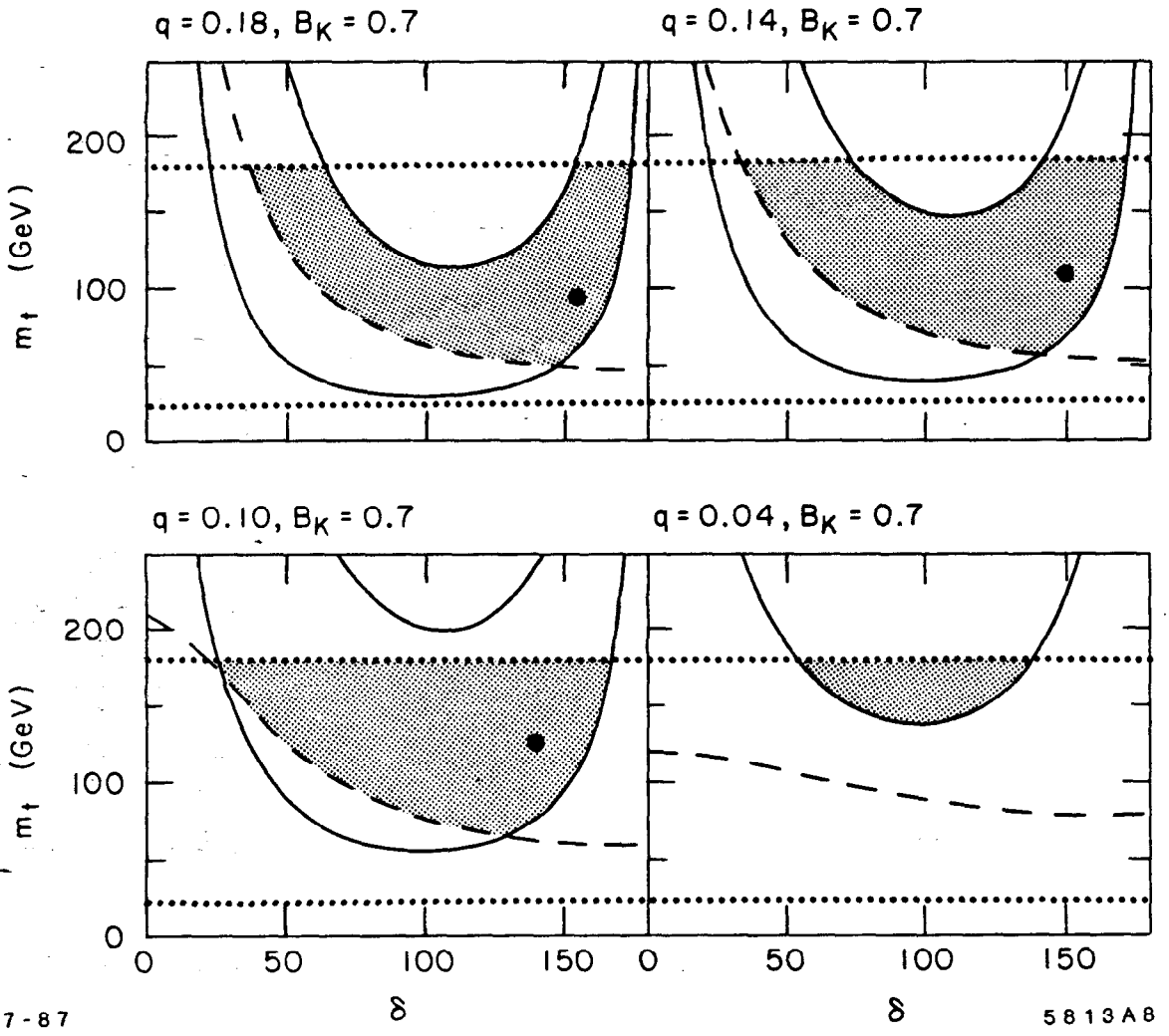
q = 0.18, B_K = 0.7
q = 0.14, B_K = 0.7
q = 0.10, B_K = 0.7
q = 0.04, B_K = 0.7
m_t (GeV)
200
100
0
0
50
100
150
δ
7-87
5813A8

Fig. 8

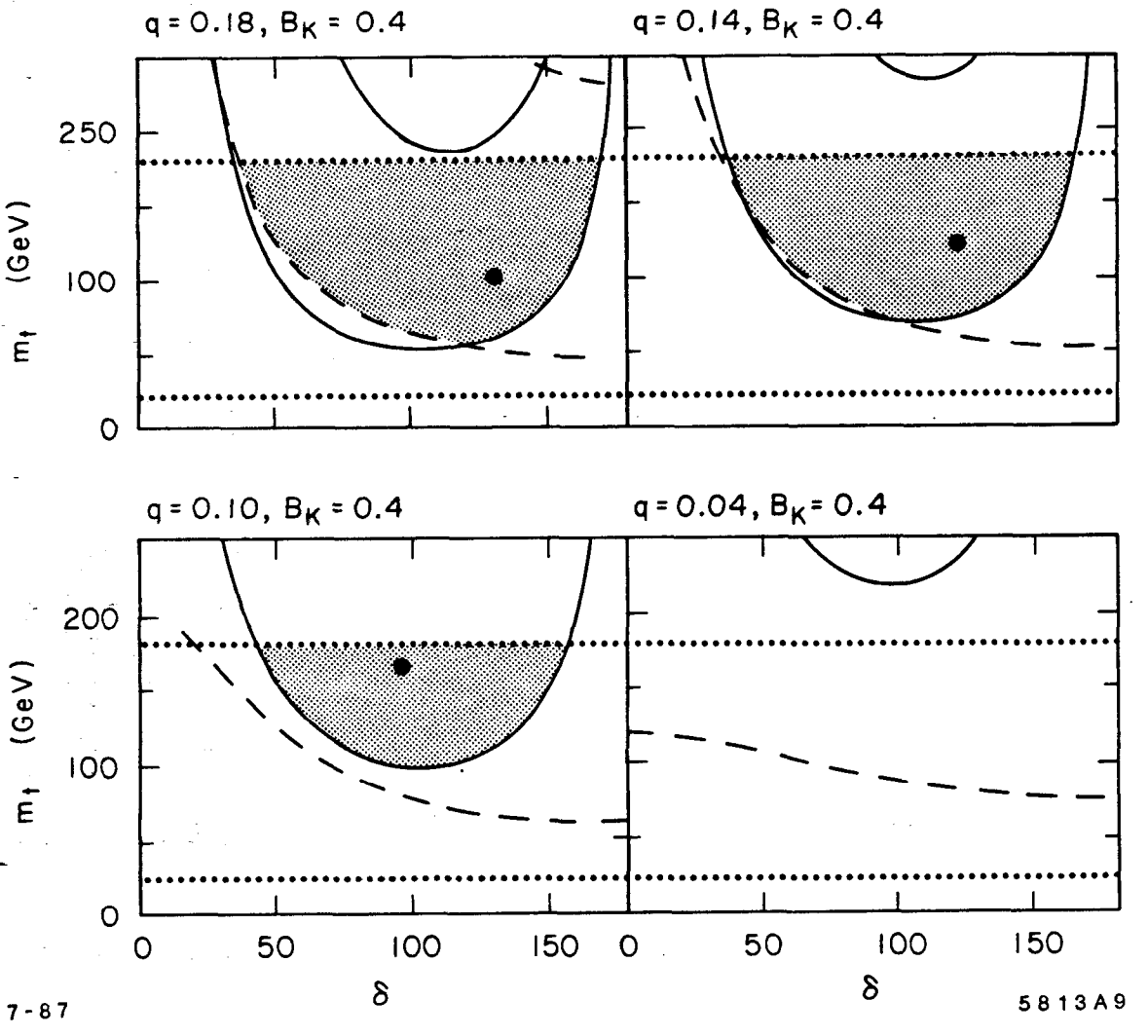
q = 0.18, B_K = 0.4
q = 0.14, B_K = 0.4
q = 0.10, B_K = 0.4
q = 0.04, B_K = 0.4
m_t (GeV)
250
200
100
0
0
50
100
150
δ
7-87
5813A9

Fig. 9

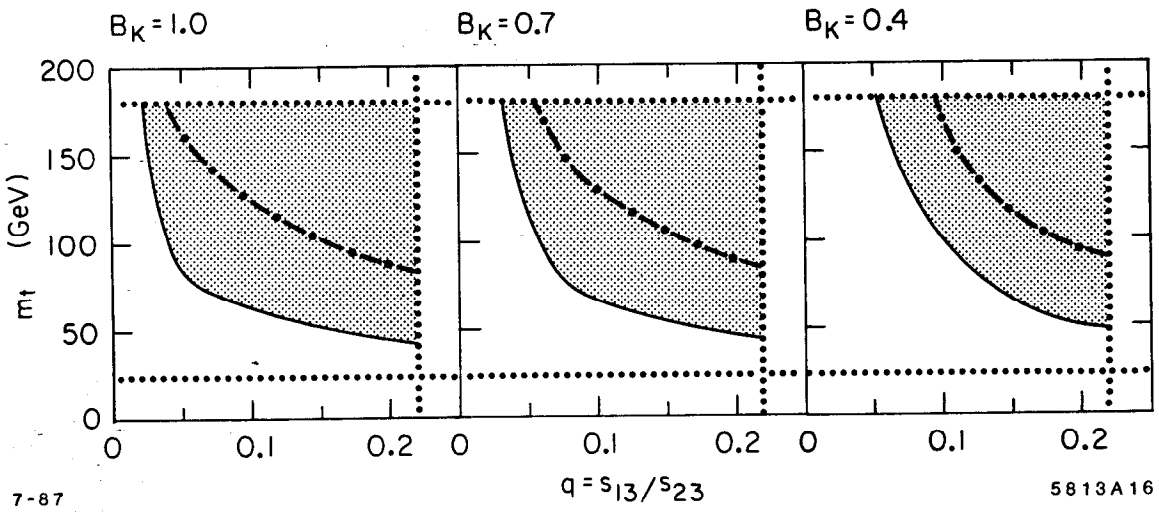
$B_K = 1.0$
$B_K = 0.7$
$B_K = 0.4$
200
150
100
50
0
m_t (GeV)
0
0.1
0.2
$q = s_{13}/s_{23}$
7-87
5813A16

Fig. 10

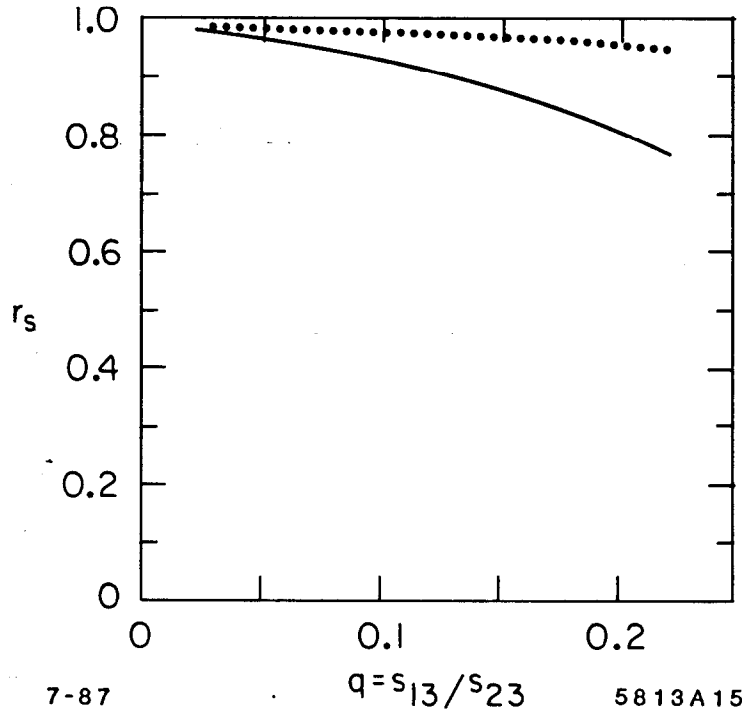

Fig. 11

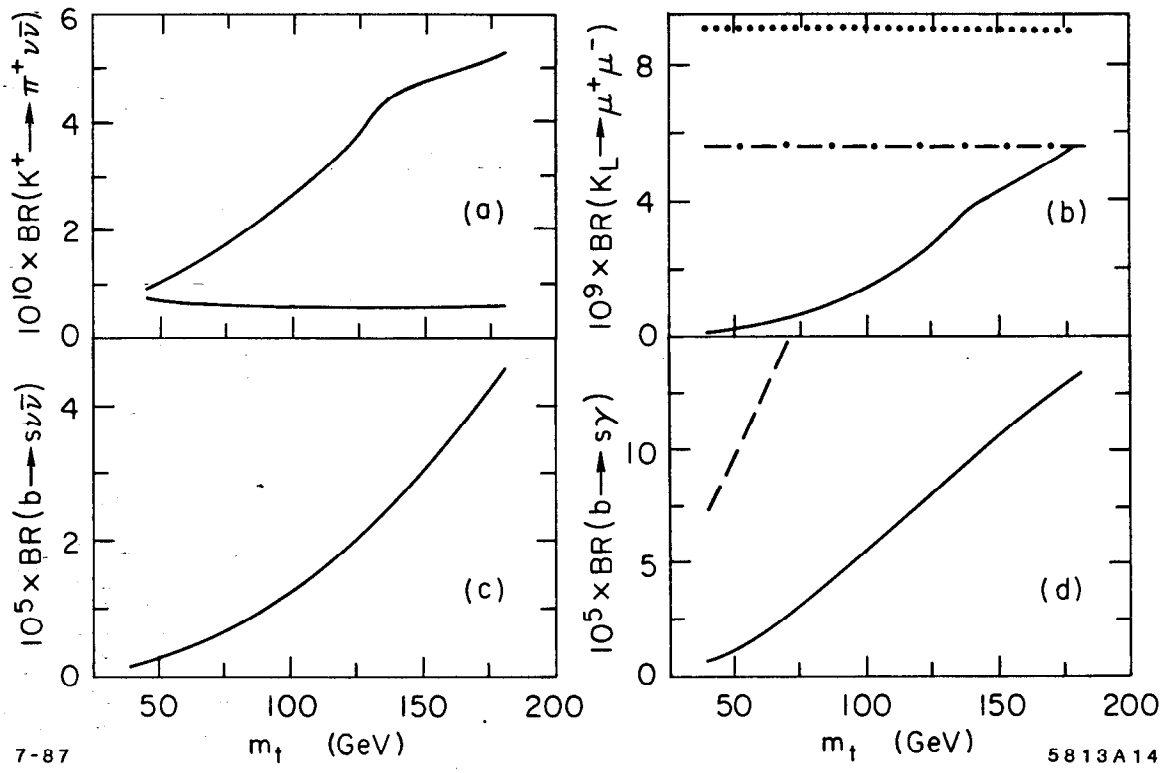
$10^{10} \times BR(K^+ \to \pi^+ \nu\bar{\nu})$
$10^9 \times BR(K_L \to \mu^+\mu^-)$
$10^5 \times BR(b \to s\nu\bar{\nu})$
$10^5 \times BR(b \to s\gamma)$
(a)
(b)
(c)
(d)
m_t (GeV)
m_t (GeV)
7-87
5813A14

Fig. 12

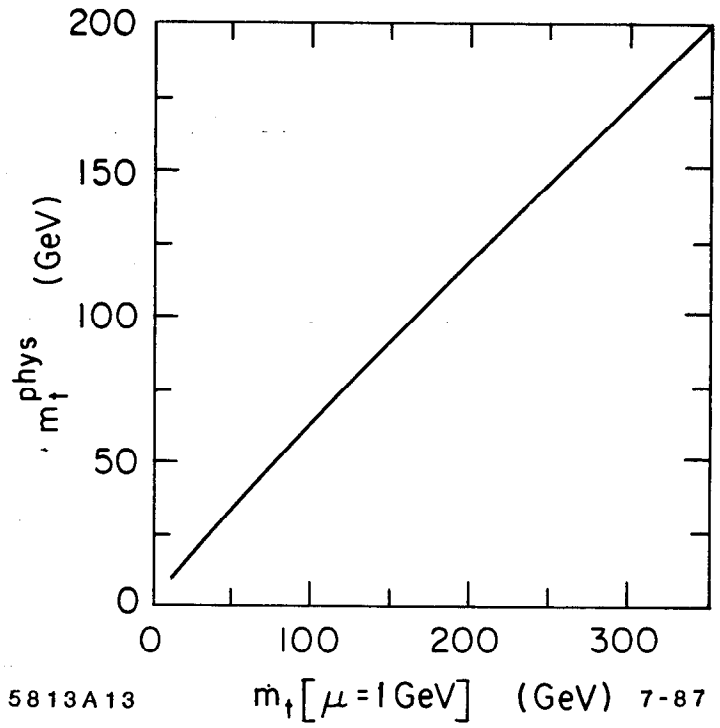
200
150
100
50
0
0
100
200
300
m_t^{phys} (GeV)
$m_t[\mu = 1\,GeV]$ (GeV)
5813A13
7-87

Fig. 13

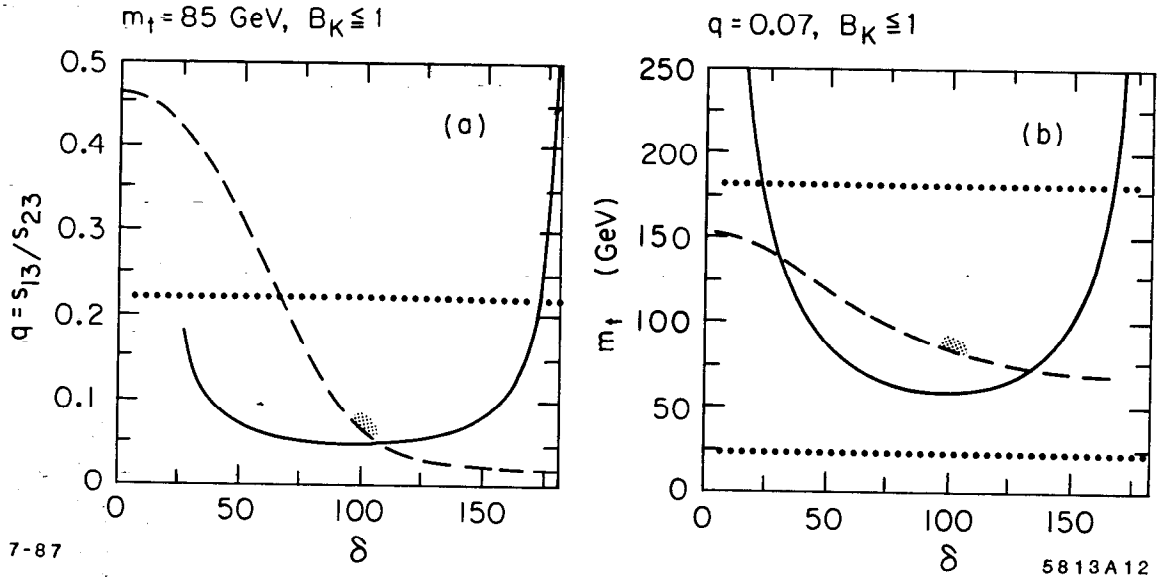
$m_t = 85$ GeV, $B_K \leq 1$
$q = 0.07$, $B_K \leq 1$
(a)
(b)
$q = s_{13}/s_{23}$
m_t (GeV)
δ
δ
0.5
0.4
0.3
0.2
0.1
0
250
200
150
100
50
0
0
50
100
150
7-87
5813A12

Fig. 14

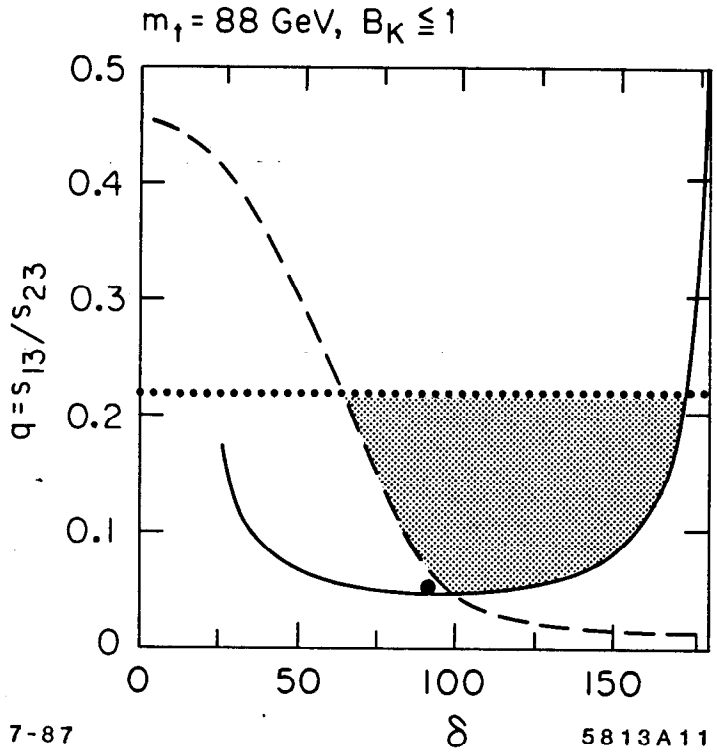
$m_t = 88$ GeV, $B_K \leq 1$
0.5
0.4
0.3
0.2
0.1
0
$q = s_{13}/s_{23}$
0
50
100
150
δ
7-87
5813A11

Fig. 15

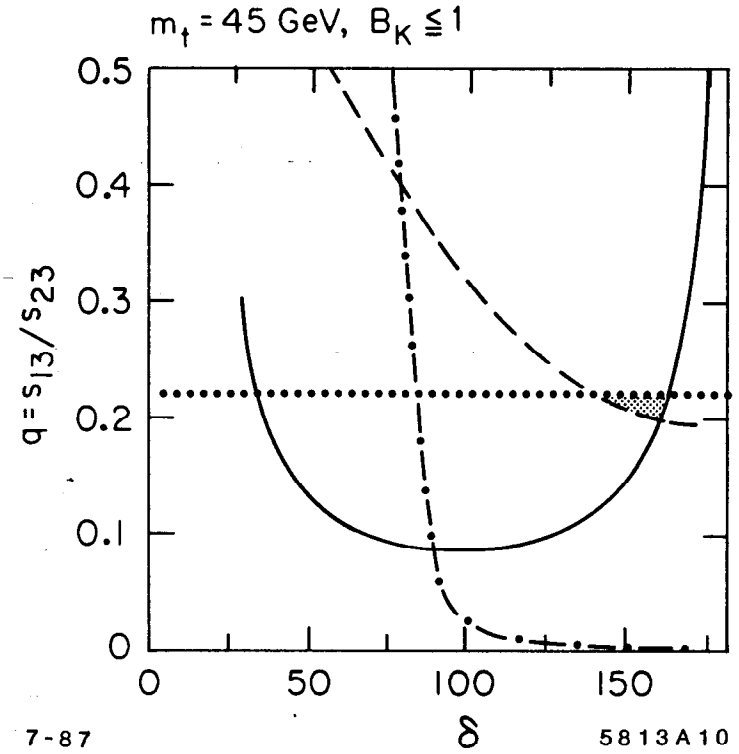
$m_t = 45$ GeV, $B_K \leq 1$
0.5
0.4
0.3
0.2
0.1
0
$q = s_{13}/s_{23}$
0
50
100
150
δ
7-87
5813A10

Fig. 16